Technische Universität Wien

Master Thesis

Screening for intrinsically hard and tough ceramic-like materials

Lukas Müllauer, BSc

supervised by
Klimashin, Fedor; Dipl.-Ing. Dipl.-Phys. Dr.techn.

co-supervised by
Holec, David; Gastprof. Mag. PhD

29th April 2019

Contents

1 Introduction

Thin film metal borides, carbides, oxides and nitrides have been studied extensively in the past 50 years. Because of their special properties such compounds have been used in a wide variety of applications, e.g. as protective coatings for tools used during milling, turning and cutting operations. Two of the most important properties determining the wear resistance of the coatings are hardness and fracture toughness. Development of new compounds combining high hardness and toughness by trial and error is generally a resource intensive process. While structures of thin films can be modelled with FEM software, intrinsic properties, e.g. elastic constants, can be calculated by DFT. Not only with elastic constants and lattice parameters on hand, intrinsic hardness and fracture toughness can be calculated, but also with properties like electronegativity, bond density, amount of bonds within a cell, coordination number and volume of unit cell. hile hardness is a well discussed and calculated value, fracture toughness is not covered as well.

The intrinsic hardness and fracture toughness of transition metal nitrides, carbides, borides and oxides will be calculated based on several semi-empirical models and compared with the experimental values available in the literature. The method that turns out as the most useful one will then be applied, to search for new hard and tough materials in an online database.

1.1 Why hard and tough materials?

In engineering applications structural materials are required to be both hard and tough, two terms in common language often used synonymously. To understand, why those properties are sought after, how hardness and strength as well as ductility and toughness are related, they must be defined [1].

- Hardness is the ability of a material to withstand local plastic deformation by a harder body.
- Strength is the maximum strain a material can withstand without plastic deformation/necking (yield strength/tensile strength).
- Ductility is the amount of deformation a material can undergo before rupture.
- Toughness is the ability of a material to absorb energy and plastically deform before fracturing

To illustrate strength and toughness a stress-strain curve from an uniaxial tensile test can be seen in fig 1.1. For the sake of completeness, two curves, apparent stress (curve

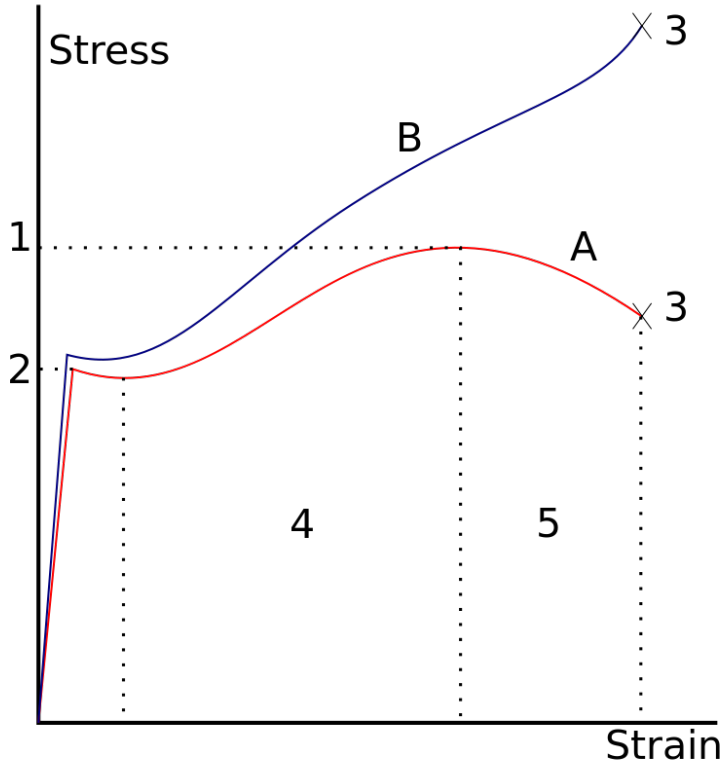

Figure 1.1: A stress strain curve with 1: tensile strength, 2: yield strength, 3: rupture, 4: strainhardening region, 5: necking region. Apparent (red) actual (blue) stress [ref. [2]].

A in fig 1.1) and actual stress (curve B in fig 1.1), are shown. During a tensile test, the specimen is suspect to forces, which change the cross-section of it. The difference in the curves, comes from the formula for stress: $\sigma = F/A$ (σ being stress, F being force, A being cross-section), where for apparent stress the initial area is used and in the actual stresses, the change in cross-section is accounted for. While strength values are distinct points on the plot, toughness is the area under the curve. Ductility can be quantified as the fracture strain e_f (strain to rupture - point 3 in fig 1.1). Hardness cannot be seen in this type of curves, as it is a property that is dependent on all three of the above, however as a rule of thumb it can be said, that $R_m(MPa) = 3.45 \cdot H$ for steels [1], for different materials, other constants apply.

A good example to further explain these relationships and how to combine the properties is using e.g. quenched and tempered steel as base material, which has high strength and toughness, reasonable ductility, but low hardness.

After this short paragraph about the basics of hardness and related properties, it is clear, how to measure strength, ductility and toughness (uniaxial tensile test), however no means to quantify hardness were introduced. While methods to do so, were already

documented by Friedrich Mohs (1773-1839), who divided materials into 10 groups, depending on their scratch resistance. Since then hardness testing came a long way, and modern tests such as Brinell, Knoop, Rockwell or Shore hardness tests, which all use indenters of different geometries to quantify the resistance to penetration into the surface of the material. For thin films nanoindentation was introduced, which works the same way, however loads are much lower, so that the indentation-depth stays in the region of 10% of film thickness, which is necessary to minimise effects of the substrate [3].

1.2 Chemical Bonding

Bond type has a strong influence on the hardness and toughness of compounds. For this purpose, two different ways to graphically distinguish between covalent, ionic and metallic bonds were tested. The first method used was the one proposed by Meek et al. (2005), based on $\Delta\chi$ (difference between the EN's of the bonding partners) and χ_{avg} (average EN of the bonding elements) based on the Pauling scale of electronegativity (EN) [4]. The result is a bond triangle, with pure ionic, pure metallic, and pure covalent bonds in the corners. The resulting triangular plots can be separated by straight lines, to distinguish between covalent, ionic and metallic regions [4]. This method gives good results for strong covalent and ionic bonds, however compounds which are close to boarders, are susceptible to errors.

The second method used was introduced by Sproul (1994), and uses total EN values [5–8]. Here the compounds are plotted in a graph, where the x-axis corresponds to the element with the higher EN and the y-axis with the lower EN. For instance NaCl ($\chi_{Na} = 0.93, \chi_{Cl} = 3.16$) can be found in the region for ionic bonds in fig 1.2b. In this plot, all metal bonds lie in a region, where the higher EN is lower than 2.2 on the Pauling scale. To distinguish between covalent and ionic bonds, a threshold of 1.7 EN units is set, where if the lower EN is higher than 1.7 the bond is covalent and ionic, if it is lower than 1.7. In this representation, compounds without transition metals can be characterised with lower error margins compared to the method proposed by Meek et al. (2005) [4]. If transition metals are introduced only the border between metallic and non metallic compounds remains intact.

However the introduced methods are not very elegant and precise solutions to distinguish bond types in transition metal compounds, and hence to predict their hardness and toughness.

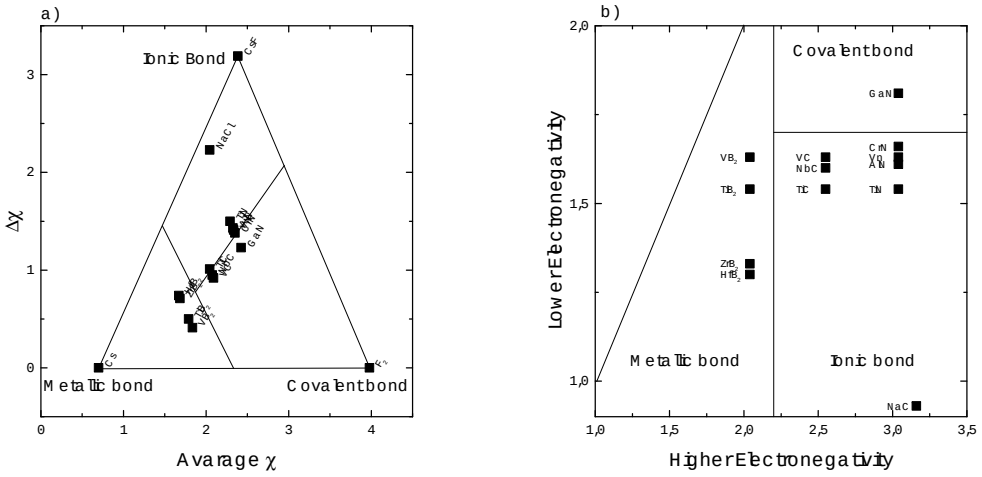

Figure 1.2: Bond triangles by a) Meek and b) Sproul of some transition metal compounds.

1.3 Mechanisms controlling hardness & toughness

This work focuses mainly on intrinsic aspects of hardness and toughness of ceramic-like materials. In this chapter, the fundamentals of intrinsic hardness and toughness will be discussed. The boundary between intrinsic and extrinsic properties appears however vague. Some properties, for instance grain size, are considered intrinsic by some authors (e.g. Wang et al. (2014) [9]) , but extrinsic by others (e.g. by Tian et al. (2011) [10]).

There are three conditions, a hard material must fulfill [11].

1. High bulk modulus
2. High shear modulus
3. Creation and motion of dislocations must be as small as possible

Regarding toughness, Wang et al. identified two points, crucial for high values [9]

1. Low shear to bulk modulus (G/B) ratio and high Cauchy pressure ($C_{12} - C_{C14}$)
2. Nano-sized grains

Finding correlations to compute hardness from intrinsic values of the material shows great difficulty and became possible only in the past 15 years. Different approaches were used, based on bond strength, bond density, number of bonds, electronegativity and elastic properties, as discussed in the previous chapter. While the different approaches might work for different types of materials, it is especially hard to find one correlation that can be applied for metallic, ionic and covalent bonds, and mixtures of those.

Another intrinsic property important for hardness and fracture toughness is ductility. It describes the behaviour of materials under tensile stresses. High ductility occurs mainly in metallic bonds, were delocalised valence shell electrons are shared between atoms, which enables the metal atoms to slide past one another.

1.3.1 Solid solution effect

Solid solution strengthening is a mechanism, that can be used to improve strength in materials, by alloying with other elements. The main and the alloying element build a solid solution, where the alloying element hinder dislocation movement due to lattice strain. Solid solution strengthening is dependent on the lattice constants of the partaking elements, the shear modulus and the volume fraction of solute atoms.

Many methods have been proposed to calculate the effect of solid solution strengthening, such as the classical Fleischer model [12], Rupert et al. (2010) [13], Leyson et al. (2012) [14], Ma et al. (2014) [15], as well as Gao (2017) [16], whoms method was used here and will be explained in the following paragraph.

Faming Gao determines the hardening stress $\Delta\tau_{cg}^{F}$ by three factors: shear modulus G, the volume fraction of solute atoms f_v and the size misfit degree δ_b, the stress in a general form can be expressed as:

$$\Delta\tau_{cg}^{F} = A \cdot G(f_v \cdot \delta_b^q)^P \tag{1.1}$$

where A, p, q are constants. The formula was fitted to KBr_xCl_{1-x} and it follows to:

$$\Delta\tau_{cg}^{F} = 0.27 \cdot G\sqrt{f_v \cdot \delta_b^{2/3}} \tag{1.2}$$

where the volume fraction of solute atoms in KBr_xCl_{1-x} ($x<0.5$) is calculated in the following way:

$$f_v = \frac{x \cdot R_{Br}^3}{[x(R_K^3 + R_{Br}^3) + (1-x)(R_K^3 + R_{Cl}^3)]} \tag{1.3}$$

and δ_b with the following formula:

$$\delta_b = \frac{da/dc}{a} \tag{1.4}$$

where a is the lattice constant and c the concentration.

Ductility

In general it is of great interest what kind of fracture behaviour a certain material exhibits. For this reason two different criteria will be utilised to distinguish between brittle and ductile materials. Pugh's modulus (G/B) ratio divides materials into brittle ($G/B > 0.571$) and ductile ($G/B < 0.571$) [17]. The Pettifor criterion utilises the Cauchy pressure [18]. When the bonding is more metallic hence ductile, the Cauchy pressure will be positive. A negative Cauchy pressure characterises covalent bonding, therefore brittle materials. The Cauchy pressure is calculated by the following formula

$$P_{cauchy} = \frac{(c_{12} - c_{66}) + (c_{13} - c_{55}) + (c_{23} - c_{44})}{3} \tag{1.5}$$

1.4 Semi-empirical models

In this section, the methods used for the calculation of hardness and fracture toughness will be discussed in chronological order.

1.4.1 Šimůnek (2007)

To use his formula [19], only a pocket calculator and some materials properties, which are easy to find, are needed. It is only dependent on coordination number n_i, interatomic distance of atoms d_{ij}, valence electron number Z_i, the radius of a sphere R_i, that contains exactly the electronic valence charge Z_i, the volume of the unit cell Ω, the number of interatomic bonds between atoms in the unit cell b_{12}, as well as constants C and σ.

$$H = \left(\frac{C}{\Omega}\right) b_{12} s_{12} e^{-\sigma f_2} \tag{1.6}$$

with

$$f_2 = \left(\frac{e_1 - e_2}{e_1 + e_2}\right)^2 \tag{1.7}$$

and

$$s_{ij} = \frac{\sqrt{(e_i e_j)}}{n_i n_j d_{ij}} \tag{1.8}$$

as well as

$$e_i = \frac{Z_i}{R_i} \tag{1.9}$$

The main advantage of this approach lies in the ease with which it can be used. All the variables are readily available. The number of interatomic bonds is dependent on the structure of the compound, the constants C and σ are fitted to experimental values and calculated to be 1400 and 2.8 respectively by Šimůnek and others [20]. This formula is valid for both *covalent* and *ionic* materials.

1.4.2 Li (2008)

Li et al. [21] computes hardness from the viewpoint of electronegativity (EN). Therefore the type of bond, which is dependent on the electronegativity difference between the bonding partners at least to some extent, is already taken into account. The overall formula to calculate Knoop hardness for covalent and polar covalent crystals can be expressed as

$$H_k(GPa) = 423.8 N_v X_{ab} e^{-2.7 f_i} - 3.4 \tag{1.10}$$

where f_i is an indicator for ionicity and is calculated according to

$$f_i = \frac{0.5 \cdot |\chi_a - \chi_b|}{2 \cdot \sqrt{\chi_a \cdot \chi_b}} \tag{1.11}$$

and X_{ab} expressing the bond electronegativity

$$X_{ab} = \sqrt{\frac{\chi_a}{CN_a} \cdot \frac{\chi_b}{CN_b}} \tag{1.12}$$

N_v is the covalent bond density, χ_i is the electronegativity in a modern EN scale called "covalent potential", CN_a is the coordination number of element a. This formula was also adapted by Oganov et al. to be used in his USPEX (Universal Structur Predictor) code. [22]

1.4.3 Chen (2011)

In this newer approach, Chen et al. [23] propose a correlation between hardness and elastic properties, which can be calculated accurately as

$$H_v = Ck^m G^n \tag{1.13}$$

where H is the Vickers hardness, G is the shear modulus and B is the bulk modulus. This ratio was already proposed in 1954 by Pugh, as a measurement of strain at fracture ($\epsilon_f \propto (B/G)^2$) ($\epsilon$ being the strain at fracture) [17]. Secondly and even more important, Pugh stated, that the ratio G/B is a measurement for brittleness and ductility of pure metals. Chen advanced this statement to correlate the hardness and elasticity in intrinsically brittle materials. The higher the G/B ratio is, the more brittle the material is. His formula (parameters fitted to different well known structures) becomes

$$H_v = 2(k^2 G)^{0.5850} - 3 \tag{1.14}$$

were k is the ratio G/B

The constants were first found to be $C = 1.887$, $m = 1.171$ and $n = 0.591$ by selecting 10 materials (diamond like: diamond, c-BN, β-SiC, Si and Ge, zinc blende: ZrC and AlN, and rocksalt structures: GaP, InSb and AlSb), because their hardness, bulk and shear moduli are well known. This first fitting was then refined, by plotting k^2G versus H_v and fitting the resulting curve to the final values of C, m and n, as well as a numerical factor of -3.

Due to the numerical factor of -3, the results can turn negative at the lower end of the hardness spectrum. This is physically not probable, therefore Tian et al. (2012) [10] revised the formula, re-fitted it without the numerical term, which results to

$$H_v = 0.92 \cdot k^{1.137} \cdot G^{0.708} \tag{1.15}$$

1.4.4 Griffith (1924),

The work of Griffith [24] in 1924 about glass, started the development of linear elastic fracture mechanics. One major outcome is the following formula, explaining the relationship between fracture toughness K_I (stress intensity factor for mode 1 crack loading), surface energy γ and Young's modulus E. The formula is still widely used in the literature e.g.: Guo et al. (2008) [25, 26].

$$K_I = \sqrt{\pi \cdot \gamma \cdot E} \tag{1.16}$$

1.4.5 Niu (2018)

By using elastic properties, namely shear and bulk modulus, Niu et al. [27] proposed a simple and accurate model of fracture toughness. Just like Chen et al. in his formula for hardness, Niu proposed a similar approach for K_IC (the critical fracture toughness). The empirical formula again follows the Pugh ratio, and the following relation

$$K_{IC} \propto G \cdot (B/G)^m \tag{1.17}$$

For the units to be correct, a length scale must be added. Volume per atom V_0 was chosen. After fitting to experimental data, the following formula for covalent and ionic crystals results

$$K_{IC} = V_0^{1/6} \cdot G \cdot (B/G)^{(1/2)} \tag{1.18}$$

In this work, for all materials the Voigt-Reuss-Hill average was used for the elastic constants (bulk and shear modulus). This average value is calculated from Voigt's upper bound and Hill's lower bound formulas [28, 29]. The procedure was chosen to provide consistent elastic constants.

1.5 Comprehensive overview

In this section the previously introduced formulas are densely compiled into one table.

Table 1.1: The four methods used to calculate hardness and fracture toughness.

Name	Formula	Parameteres	valid for
Šimůnek (2007)	$H = \left(\frac{C}{\Omega}\right) b_{12} s_{12} e^{-\sigma f_2}$	Bond strength, number of bonds, volume of unit cell	Cases, where the bond charge lies between atoms
Li (2008)	$H = 423.8 N_v X_{ab} e^{-2.7 f_i} - 3.4$	Electronegativity and bond density	Polar covalent and covalent bonds
Chen (2011)	$H = 2(k^2 G)^{0.5850} - 3$	elastic properties	Ductile and brittle materials
Griffith (1924)	$K_I = \sqrt{\pi \cdot \gamma \cdot E}$	Youngs modulus and surface energy	–
Niu (2018)	$K_{IC} = V_0^{1/6} \cdot G \cdot (B/G)^{(1/2)}$	elastic properties and volume per atom	covalent and ionic crystals

The formulas by Šimůnek and Li, while having different approaches in physical treatment, both are based on the assumption, that the hardness correlates with the sum of the resistances of each chemical bond to the indentation per unit area. The differences are, that the resistances are formulated by the bond strength (Šimůnek) and electronegativity (Li). These models work well for pure covalent and polar covalent bonds, as soon as some form of metallic bond is introduced to the compound, these models cannot correctly reproduce hardness values any more. On the other hand the formula by Chen fails to reproduce hardness values for ionic crystals.

Therefore it can be summed up, that the methods complement each other well, and in general, depending on the compound, one has to choose the most applicable method.

2 Evaluation of hardness and fracture toughness of binary nitrides, carbides, borides and oxides

In this chapter, hardness and fracture toughness of binary compounds were calculated using different approaches (see chapter 1.5) and compared with literature values. These materials are well researched experimentally and theoretically and the mentioned methods can be well evaluated. Certain strengths and weaknesses of different formulas can be seen easily and knowledge of these can then be applied in more advanced ternary phases.

In general, a high hardness is sought after, although very hard materials tend to be brittle [30]. Therefore a balance between hardness and also fracture toughness is the holy grail of new high-performance materials.

As discussed before, the type of chemical bonding is a major factor, when asked for materials properties such as hardness, strength or ductility. Therefore in the following chapters, the four compound groups will be discussed according to their predominant bond types, which can be seen in fig 2.1.

In the following sections some of the used parameters are tabulated (elastic properties and lattice parameter), while others are readily tabulated elsewhere (covalent radii [31], number of valence electrons [32] and number of bonds in a unit cell [19, 33]).

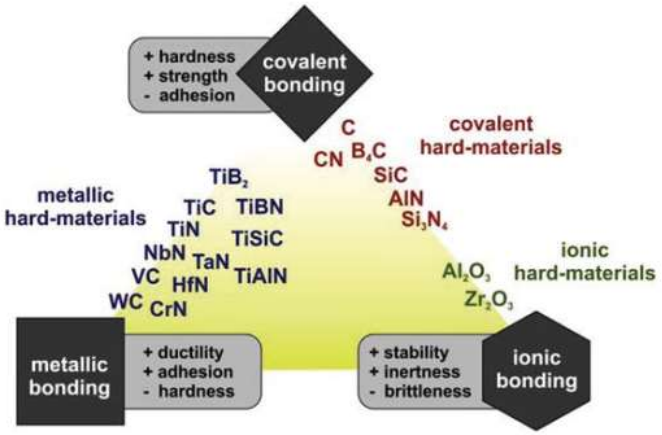

Figure 2.1: Bond triangle with representative compounds, taken from Mayrhofer et al. [34].

2.1 Nitrides

Transition metal nitrides are widely used in the fields of e.g. catalysis, tooling, optics, decoration and semiconductors. Some specific applications are shown by VN in super capacitors, TiN in cutting tools and as decorative or optical coatings, ZrN and HfN in concentrating solar collectors as well as AlN, GaN and InN which are used in semiconductors. In general groups 3, 4, 5 and 6 form nitrides with high melting points and high chemical stability. Group 7 and 8 transition metal nitrides decompose readily. The elastic properties [35–44], lattice constants [45], covalent radii [31] were taken from various literature sources.

Table 2.1: Elastic properties of the investigated nitrides in spacegroup number 225, unless specified otherwise. Bold compounds were used for further calculations.

Compound	C_{11}	C_{12}	C_{44}	a (Å)	source
AlN	418	169	308	4.07	[42]
ScN	388	106	166	4.52	[42]
TiN	575	130	163	4.25	[42]
TiN	561	122	160	4.27	[43]
TiN	585	122	163	4.25	[46]
VN	660	144	120	4.13	[42]
VN	581	183	123	4.12	[46]
CrN	524	113	118	4.13	[35]
CrN	572	209	6	4.05	[46]
CrN	580	210	8	4.14	[47]
GaN (186)	344	134	90	3.24	[36, 48]
YN	318	81	124	4.92	[42]
YN	319	84	122	4.89	[37]
ZrN	462	141	143	4.57	[44]
ZrN	523	111	116	4.62	[42]
ZrN	563	101	122	4.58	[37]
ZrN	521	114	110	4.60	[46]
NbN	649	136	80	4.43	[42]
NbN	692	141	143	4.41	[44]
NbN	685	121	79	4.42	[46]
NbN	722	108	88	4.41	[37]
RhN	462	198	56	4.35	[44]
PdN	345	178	50	4.40	[44]
AgN	231	120	30	4.59	[44]
LaN	198	86	71	5.31	[42]
HfN	588	113	120	4.54	[42]
HfN	580	116	114	4.54	[46]
HfN	705	112	131	4.44	[49]
TaN	715	138	60	4.43	[42]
TaN	750	122	62	4.42	[46]
TaN	901	109	60	4.31	[43]
TaN	827	156	73	4.33	[49]
WN_2 (123)	853	122	203	2.67	[39]
PtN	285	223	45	4.50	[44]

Unstable compounds, with negative elastic constants, were not taken into account. The elastic properties were used to calculate hardness after Chen(2011), and fracture toughness after Niu(2018). In Table 2.2, for each compound only one set of elastic properties are shown, to keep the table short and comprehensive. For most of the compounds

far more than one set of elastic properties are available. In this work, only constants computed with GGA (Generalised gradient approximation) were taken into account. In table 2.2 all the found stiffness tensors c_{ij} are shown, however for further calculations only the ones in bold are considered.

In fig 2.2 all the calculated values can be compared. It can be seen, that there are very big differences between the methods used, to calculate the values. Some values agree well with experimental results, others are unrealistically high, as can be seen in fig 2.2. The bond density method by Li overestimates the hardness of transition metal nitrides the more, the more *d* electrons are available, with the exception of AgN, because it has a fully filled *d* shell and only one valence electron in an *s* shell. This general behaviour might stem from the assumption in this formula, that all bonds are covalent.

The hardness calculated with the formula proposed by Šimůnek seems to produce realistic values, although they do not always agree well with the ones computed with the formula by Chen. Reason for this behaviour could be, that the model by Šimůnek works well for pure covalent and polar covalent crystals. The model by Chen et al. gives a good idea about the expected hardness in intrinsically brittle materials, therefore compounds with a high degree of metal bonds tend to be over- or underestimated by this formula.

Table 2.2: Calculated and experimental hardness values of binary nitrides

Compound	H_C	H_S	H_L	Exp	K_{IC-N}	$K_{G\ -[100]}$	$K_{G\ -[110]}$
AlN	40.4	18.6	36.9	-	3.5	1.2	2.3
AlN (wurtzite)	14	–	–	18^{1}; 12 $\pm$1 [1][50, 51]	–	–	–
ScN	24.8	7.2	15.5	–	2.7	–	–
TiN	23.7	11.8	32.3	22^{2}; 21^{1}[52]	3.3	1.5	1.7
VN	18.2	15.8	51.1	15$\pm$1 [1]; 13^{1}[51, 52]	3.4	1.3	1.5
CrN	17.5	20	76.8	15 [2],11^{1}[52, 53]	2.7	1.1	1.0
GaN	9.9	30.4	54.9	12$\pm$2[1][51]	1.9	–	–
YN	20.2	4.3	9.2	–	2.2	–	–
ZrN	18.5	7.4	21.5	16 [2][52]	3.0	1.7	1.7
NbN	14.3	10.8	37.2	24^{2},14$\pm$1 [1][52, 51]	3.2	–	–
RhN	5.5	14.3	99.3	–	2.3	–	–
PdN	3.9	13.2	108.5	–	1.8	–	–
AgN	2.6	5.2	1	–	1.2	–	–
LaN	8.5	2.8	5.5	-	1.5	–	–
HfN	19.9	7.9	22.8	21^{2}; 17$\pm$2[1][52, 51]	3.2	1.9	1.8
TaN	13.2	10.3	35.4	10^{13}[52]	3.3	–	–
WN_2	33.8	70.1	186	–	3.6	–	–
PtN	1.6	12,2	100.8	–	1.5	–	–

[1] bulk material
[2] thin film
[3] hexagonal component

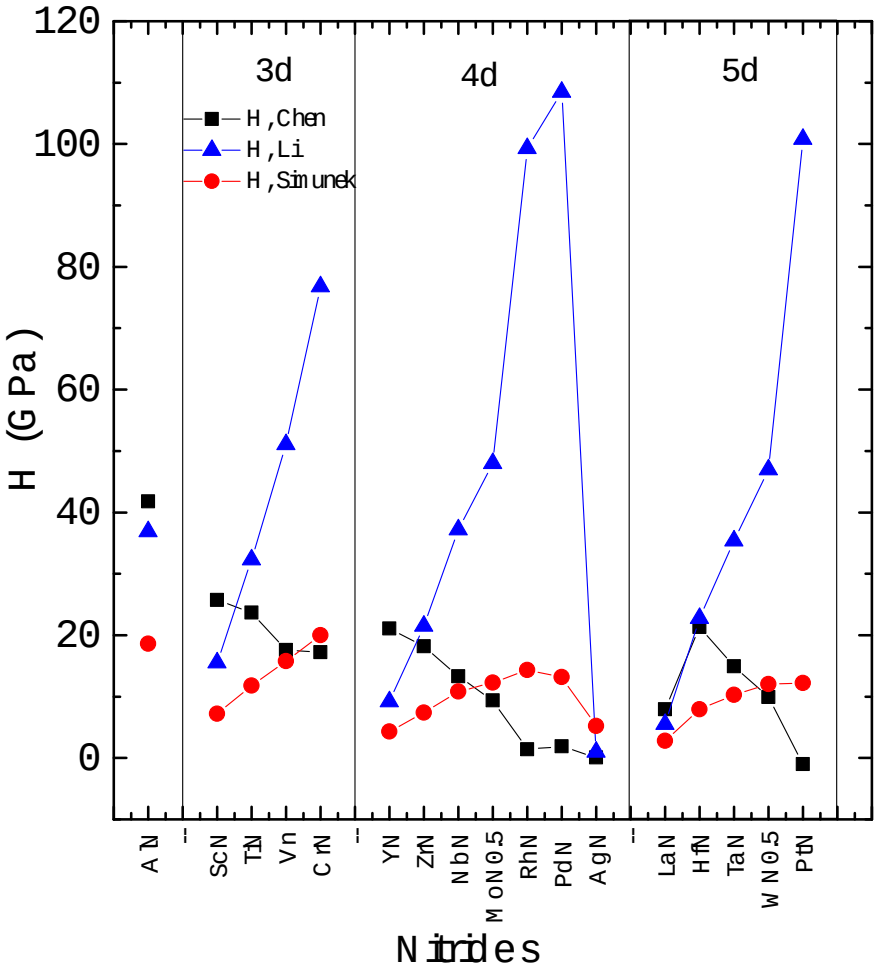

Figure 2.2: Calculated hardness values of transition metal nitrides.

2.2 Carbides

Carbides, especially WC and TiC are widely used as coatings in cutting tools. Other carbides, like SiC, are used as microelectronics and microelectromechanical systems. Nickel-based carbides have been used in ultra large scale integrated circuit devices for preparing low resistivity Ni - silicide contacts, furthermore NiC is used as catalyst and therefore thin films on chemical reactors are of great interest.

The elastic properties used for the subsequent calculations are tabulated in table 2.3. Similarly, the hardness and fracture toughness were calculated by implementing the methods of Šimůnek (2007), Li (2008), Chen (2011), Griffith 1924 and Niu (2018). The results can be seen in table 2.4, as well as in fig 2.3. For the hardness calculations only elastic properties marked in bold were used.

In the case of TiC, depending on the constants used, the hardness values calculated with Chen's formula range from 25.6 GPa to 40.2 GPa. These results show a major drawback of the method, namely, it is very dependent on the elastic constants used. For TiC 4 different sets of elastic constants were used to calculate hardnesses, to show this dependency. Three out of the four calculated numbers lie in the range 25 - 30 GPa, which corresponds well to experimental values. However the calculated hardness of 40.2 GPa is 30% too high. This shows, that for realistic elastic constants, the model works very well.

In transition metal carbides, hardness according to Šimůnek constitutes a lower limit. Hardness values determined with the formula by Chen give a good idea about the to be expected hardness in intrinsically brittle materials. Therefore compounds with a high degree of metal bonds tend to be over or underestimated by the formula of Chen. It can be seen, that the hardnesses computed with the formula by Li agree well with the others, if the compounds are mainly covalent, if not, Li strongly overestimates the hardnesses. Therefore hardnesses calculated by this formula need to be treated with care.

Table 2.3: Elastic properties of the investigated carbides.

Compound	C_{11}	C_{12}	C_{44}	a (Å)	source
TiC	513	106	178	4.33	[54]
TiC	472	99	159	4.33	[55]
TiC	500	113	175	-	[56]
TiC	418	89	217	4.33	[54]
TiC	507	121	172	4.33	[57]
TiC	610	124	173	4.33	[58]
VC	783	131	196	4.14	[58]
$VC_{0.83}$	366	110	192	-	[54]
ZrC	452	107	155	4.68	[57]
ZrC	462	102	154	4.68	[59]
ZrC	441	60	151	4.68	[54]
NbC	604	146	179	4.46	[60]
$NbC_{0.9}$	413	111	206	-	[54]
$NbC_{0.865}$	566	117	153	-	[54]
MoC	625	181	118	4.36	[61]
HfC	527	107	160	4.64	[57]
$TaC_{0.9}$	505	73	79	4.42	[54]

Table 2.4: Hardnesses of the investigated carbides.

Compound	H_C	H_S	H_L	Exp	$K_{IC\text{-}N}$	$K_{G\ \text{-}[100]}$	$K_{G\ \text{-}[110]}$
TiC	29	15.2	32.2	25-30[1][62]	3.4	–	–
TiC	40.2	15.2	32.2	25-30[1][62]	2.9	–	–
TiC	26.5	15.2	32.2	25-30[1][62]	3.5	–	–
TiC	25.6	15.2	32.5	25-30[1][62]	3.4	1.7	–
VC	30.8	20.8	53.1	–	–	2.3	
$VC_{.83}$	30	–	–	–	–	–	–
ZrC	24.1	9.7	21.8	–	3.2	1.9	–
NbC	24.5	14.1	38	24, 24,1[1][60]	3.6	2.1	–
$NbC_{0.9}$	32.9	–	–	24, 24.1 [60]	–	–	–
$NbC_{0.865}$	23.8	–	–	24. 24.1[60]	–	–	–
MoC	13.7	13.5	42.9	21 [3][61]	3.4	–	–
HfC	25.8	10.1	22.5	–	3.5	2.0	–
$TaC_{0.9}$	16.9	13.9	37.2	21 [61]	2.5	–	–
WC	17.9	15.7	51.2	13[1][63]	3.9	–	–

[1] bulk material
[2] thin film
[3] calculated

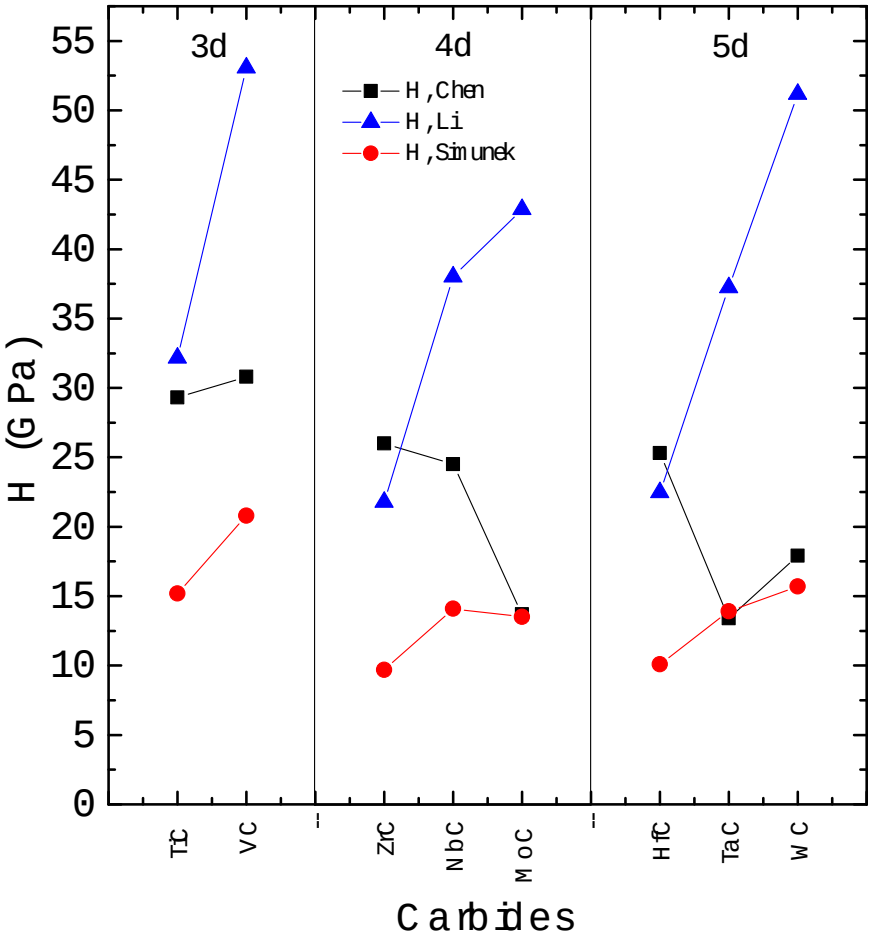

Figure 2.3: Calculated hardness values of transition metal carbides.

2.3 Borides

Borides are widely used as hard ceramic coatings, in cutting tools, but also as coatings with high thermal stability for application in high-temperature environments [64]. Diborides have been investigated in the 1970s, and applied for mechanical, thermal, or optical reasons since then. Most of the diborides crystallise in a hexagonal structure, therefore the hardness was calculated for this structure type. The elastic constants can be seen in table 2.5. Compounds with negative elastic constants were neglected.

The calculated hardness values can be seen in table 2.6. In general the α type structure (spacegroup number 191, P6/mmm) is harder than the ω type structure (spacegroup number 194, $P6_3/mmc$).

When comparing the different methods used, the big differences can be seen in fig 2.4. For the elements Sc, Y, Zr and Hf the differences between the methods by Chen and Šimůnek are moderate. For the other computed elements the differences are substantially. In the following paragraphs, the trends and values of the graph will be discussed.

The first point that stands out in this graph (fig 2.4), is that the hardness by Li vastly overestimates some of those compounds. The hardest material known to date is diamond with a hardness of about $H_v = 100$ GPa[51]. Assuming that the values predicted by the Li method are correct, CrB_2 and MnB_2 would be roughly twice as hard as diamond. The overestimation might stem from the prerequisite of Li's formula to only use materials with mainly covalent bonds. A second error margin is the amount of electrons available to form bonds. The late transition metals have a lot of valence electrons, which is a factor in Li's formula, but most certainly not all of those contribute to the bonding.

Secondly, the good agreement of Šimůnek and Chen in groups IIIB to VB transition metal diborides (TMDB) is easy to spot. According to Fig 2.4 the hardness after to Šimůnek is very high, with all values being above 25 GPa (except the values of the cubic HfB). While this might be reasonable for the groups 3B to 6B TMDB, it seems very unlikely to be true for later ones. This might stem from the amount of valence electrons contributing to the bond strength calculated in the formula by Šimůnek. The high number of valence electrons present in late transition metals skew the hardness values to unreasonable high values.

For those reasons, the hardness values calculated by Chen's formula provide the most trustworthy values over a wide range of compounds.

Table 2.5: Elastic properties of the investigated diborides in α type structure (191) and in ω type structure (194).

Compound	C_{11}	C_{12}	C_{13}	C_{33}	C_{44}	C_{66}	a (Å)	c (Å)	source
α -ScB_2	492	35	41	342	185	228	3.15	3.53	[65]
ω -ScB_2	344	43	82	0	38	150	3.14	15.42	[65]
α -TiB_2	638	59	75	392	256	289	3.04	3.23	[65]
ω -TiB_2	491	138	87	527	156	176	3.02	14.29	[65]
α -VB_2	662	109	94	426	223	277	3.00	3.03	[65]
ω -VB_2	538	89	92	514	236	225	2.94	13.44	[65]
α -CrB_2	563	135	57	366	163	214	2.97	3.00	[65]
ω -CrB_2	572	115	84	591	230	229	2.91	12.85	[65]
α -MnB_2	457	233	211	182	155	112	2.99	2.85	[65]
ω -MnB_2	475	154	155	470	209	160	2.93	12.33	[65]
α -FeB_2	441	201	158	136	101	120	3.03	2.82	[65]
ω -FeB_2	486	139	129	306	173	174	2.96	12.25	[65]
α -CoB_2	515	210	131	286	61	153	3.01	2.81	[65]
ω -CoB_2	474	180	132	538	170	147	3.01	11.66	[65]
ω -NiB_2	396	152	111	260	68	122	2.96	12.69	[65]
α -ZnB_2	358	157	40	229	1	100	3.06	3.40	[65]
α -YB_2	353	49	52	312	157	152	3.30	3.87	[65]
ω -YB_2	312	30	-5	0	99	141	3.24	17.13	[65]
α -ZrB_2	548	43	89	384	246	252	3.18	3.56	[65]
ω -ZrB_2	359	100	81	414	84	129	3.16	15.63	[65]
α -NbB_2	570	97	158	370	217	236	3.11	3.32	[65]
ω -NbB_2	544	117	97	581	239	213	3.06	14.69	[65]
α -MoB_2	599	123	167	410	138	238	3.03	3.33	[65]
ω -MoB_2	567	117	127	620	221	225	3.02	13.97	[65]
α -TcB_2	570	179	118	460	52	195	2.97	3.42	[65]
ω -TcB_2	526	136	139	548	135	195	2.99	13.86	[65]
α -RuB_2	419	252	161	350	16	83	3.03	3.29	[65]
α - RhB_2	447	205	125	337	14	121	3.09	3.22	[65]
ω -PdB_2	307	164	71	215	1	71	3.03	14.74	[65]
α **-HfB_2**	591	50	88	412	261	271	3.15	3.49	[65]
α -HfB_2	595	80	141	437	259	258	3.16	10.91	[66]
ω - HfB_2	405	102	81	449	120	152	3.14	15.33	[65]
HfB (225)	419	60	–	–	68	–	4.86	–	[66]
α -TaB_2	578	125	169	385	209	226	3.10	3.42	[65]
ω - TaB_2	558	115	95	586	247	221	3.05	14.65	[65]
α **-WB_2**	596	143	194	365	121	226	3.02	3.38	[65]
α -WB_2	586	184	235	419	95	203	3.05	3.32	[67]
ω **- WB_2**	651	170	190	680	252	240	3.03	14.07	[65]
ω - WB_2	571	145	200	672	202	212	3.04	13.84	[67]
ω **- ReB_2**	668	137	148	1063	273	266	2.88	7.41	[67]
ω - IrB_2	315	197	254	695	126	59	3.07	7.07	[68]

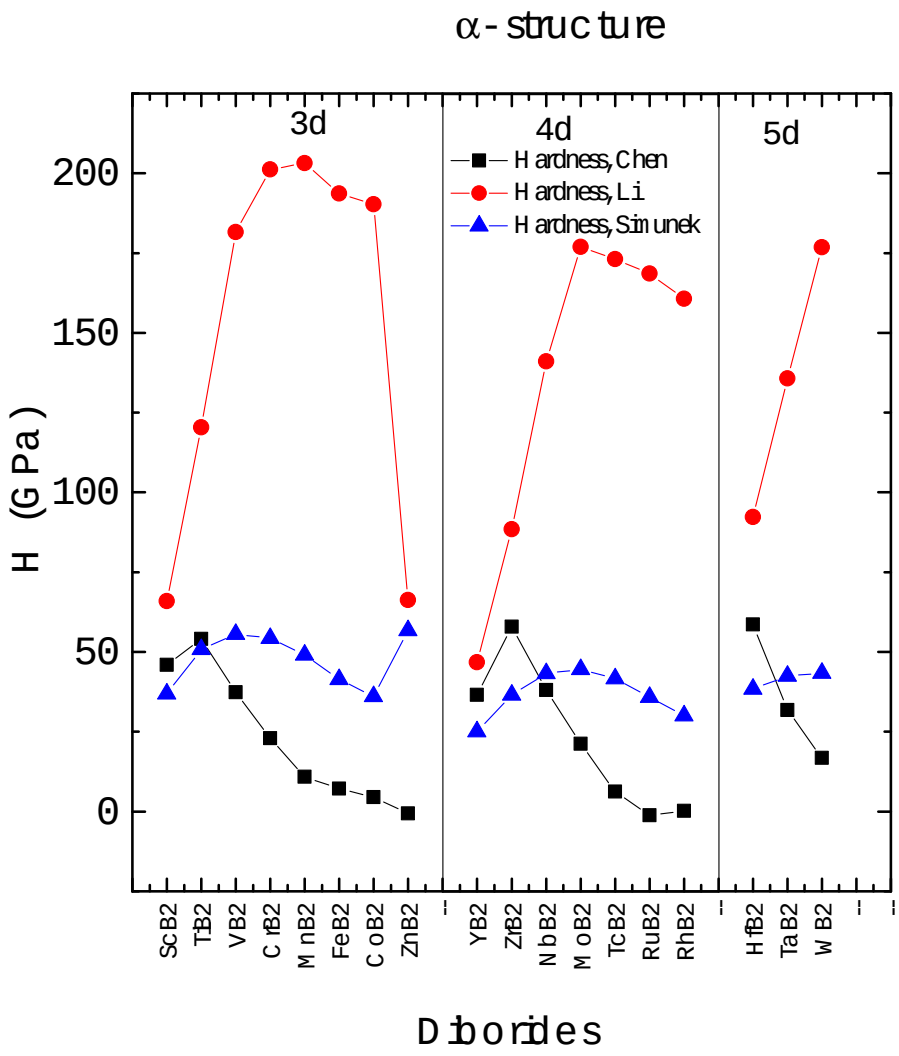

Figure 2.4: Calculated hardness values of transition metal diborides in the α-structure.

Table 2.6: Hardnesses of of the investigated diborides.

Compound	H_C GPa	H_S GPa	H_L GPa	Exp	$K_{IC\text{-}N}$ MPa$\sqrt{m}$	$K_{G\text{ -[100]}}$ MPa$\sqrt{m}$	$K_{G\text{ -[110]}}$ MPa$\sqrt{m}$
α - ScB_2	49.5	36.9	65.9	–	3.1	–	–
ω - ScB_2	11.8	8.5	12.6	–	2.2	–	–
α- TiB_2	55.1	50.8	120.4	34,32[3]; 35,[1][69, 70, 62]	3.3	–	–
ω - TiB_2	26.5	11.7	24.9	34, 32[3], 35 [69, 70]	1.8	–	–
α - VB_2	42.4	55.6	181.6	–	2.7	–	–
ω - VB_2	44	13.3	40	–	1.6	–	–
α - CrB_2	33.4	54.3	201.2	17[1][70]	2.6	–	–
ω - CrB_2	41.1	13.5	46.4	17[1][70]	1.9	–	–
α- MnB_2	8.7	49.1	203.2	7.5[1][71]	2.8	–	–
ω - MnB_2	23.8	12.1	46.4	–	1.4	–	–
α - FeB_2	7.8	41.4	193.6	–	2.0	–	–
ω - FeB_2	23.2	10.2	44.1	–	1.3	–	–
α- CoB_2	9.2	36.1	190.3	–	1.7	–	–
ω - CoB_2	20.4	8.7	43.3	–	1.3	–	–
ω - NiB_2	2.1	7.2	39.8	–	2.5	–	–
ω - NiB_2	9.4	7.2	39.8	–	2.2	–	–
α - ZnB_2	5.7	56.8	66.3	–	2.5	–	–
α - YB_2	35.8	25	46.8	–	3.4	–	–
ω - YB_2	45.4	6	8.4	–	2.5	–	–
α - ZrB_2	50.6	36.5	88.5	23 , 21[3][69, 70] , 15[1][70]	3.5	–	–
ω - ZrB_2	16.2	8.5	17.8	23, 21[3][69, 70] , 15[1][70]	2.3	–	–
α - NbB_2	31.8	43.3	141	–	3.1	–	–
ω - NbB_2	39.3	10.3	30.5	–	1.5	–	–
α - MoB_2	21.7	44.6	176.9	–	1.7	–	–
ω - MoB_2	34.4	10.7	39.9	–	1.4	–	–
α - TcB_2	13.4	41.6	173.1	–	2.6	–	–
ω - TcB_2	21	10.1	39.6	–	2.5	–	–
α - RuB_2	1.4	35.8	168.6	19.9[72]	–	–	–
α - RhB_2	4.5	30	160.7	13.6	–	–	–
ω - PdB_2	1.9	6.1	33	–	2.6	–	–
α - HfB_2	53.5	38.4	92.3	28[1]; 24, 38[69, 70]	3.4	–	–
ω - HfB_2	22.4	8.8	18.5	28[1]; 24, 38 [69, 70]	2.5	–	–
HfB (225)	15.4	18.4	30.2	–	–	–	–
α - TaB_2	27.8	42.5	135.7	25 [1][70]	–	–	–
ω - TaB_2	41.3	10.1	29.3	–	1.5	–	–
ω - WB_2	16.8	43.4	176.8	43±5	–	–	–
ω - WB_2	30.6	10.4	39.8	–	–	–	–
ω - ReB_2	40.3	21	83.6	37[1][73, 69]	–	–	–
ω - IrB_2	0.2	7.2	34.3	–	–	–	–

[1] bulk material
[2] thin film
[3] single crystal

2.4 Oxides

Transition metal oxides have a wide range of applications, e.g. TiO_2 as colour pigment, WO_3 in gas sensors or as fireproofing material or VO_2 as a infrared absorbing window coating. The conducting or semiconducting properties of many oxides are used in a wide range of applications such as photovoltaics, display technology etc. Transition metal oxides are also used as thin films, for instance Cr_2O_3 coatings for abrasion and wear resistance. Thin films of Al_2O_3 prove to be very dense and inhibit oxidation in steels with more than 5 wt.% aluminium.

The used elastic properties can be seen in Table 2.7. The calculated values can be seen in table 2.8 as well as in fig 2.5. One thing that is apparent also in the oxides, is that the hardness calculated by Li's method is overestimated for the groups 6B - 11B transition metals. It can also be seen that some of the hardness values are negative, which is physically not possible. It is hardly possible to compare the results between the methods, as they scatter. The few that produce similar values seem to agree with experimental data, e.g. TiO_2 with calculated values of 6-7 GPa (Chen and Šimůnek) and 24 GPa (Li) with experimental values ranging from 7 - 20 GPa. Other compounds like NiO, where Chen's and Šimůnek's methods seem to agree very well, do not agree with experimental values: 14 GPa in the calculated results versus 4.8-7.3 GPa.

Table 2.7: Elastic properties of the investigated oxides, in spacegroup number 225 unless specified otherwise.

Compound	C_{11}	C_{12}	C_{44}	a (Å)	source
ScO	249	138	138	–	[74]
TiO_2 (62)	619	218	52	4.52	[75]
VO	273	210	210	–	[74]
CrO	269	188	188	–	[74]
MnO	227	116	78	4.44	[74, 54]
CoO	260	145	82,4	4.26	[74, 54]
NiO	225	95	110	4.16	[74, 54]
Cu_2O	121	105	12,1	4.27	[54]
Y_2O_3 (206)	243	126	85	10.59	[76]
ZrO_2	520	93	61	–	[77]
ZrO_2 (215)	515	101	65	5.12	[78]
Reo_3 (62)	479	-7	61	-	[54]

Table 2.8: Hardnesses of the investigated oxides.

Compound	H_C	H_S	H_L	Exp	$K_{IC\text{-}N}$	K_G
ScO	17.2	–	–	–	–	–
TiO_2	6,1	6.72	24.3	7-20 [1][79]	3.0	–
VO	16.7	–	–	–	–	–
CrO	15.9	–	–	–	–	–
MnO	6.4	9.46	55.3	2.7[1][80]	1.5	–
CoO	5.3	12.65	92.8	2.8[1][80]	1.7	–
NiO	14.5	13.98	115.3	4.8-7.3[1][80, 81]	1.6	–
Cu_2O	-2.5	12.88	124.9	1.7[1][82]	0.5	–
Y_2O_3	6.9	0.15	-2.3	–	2.6	–
ZrO_2	12.4	–	–	–	3.6	–
ZrO_2	12.8	3.53	13.5	–	–	–
ReO_3 (perovskite)	26.5	–	–	–	–	–

[1] bulk material
[2] thin film
[3] single crystal

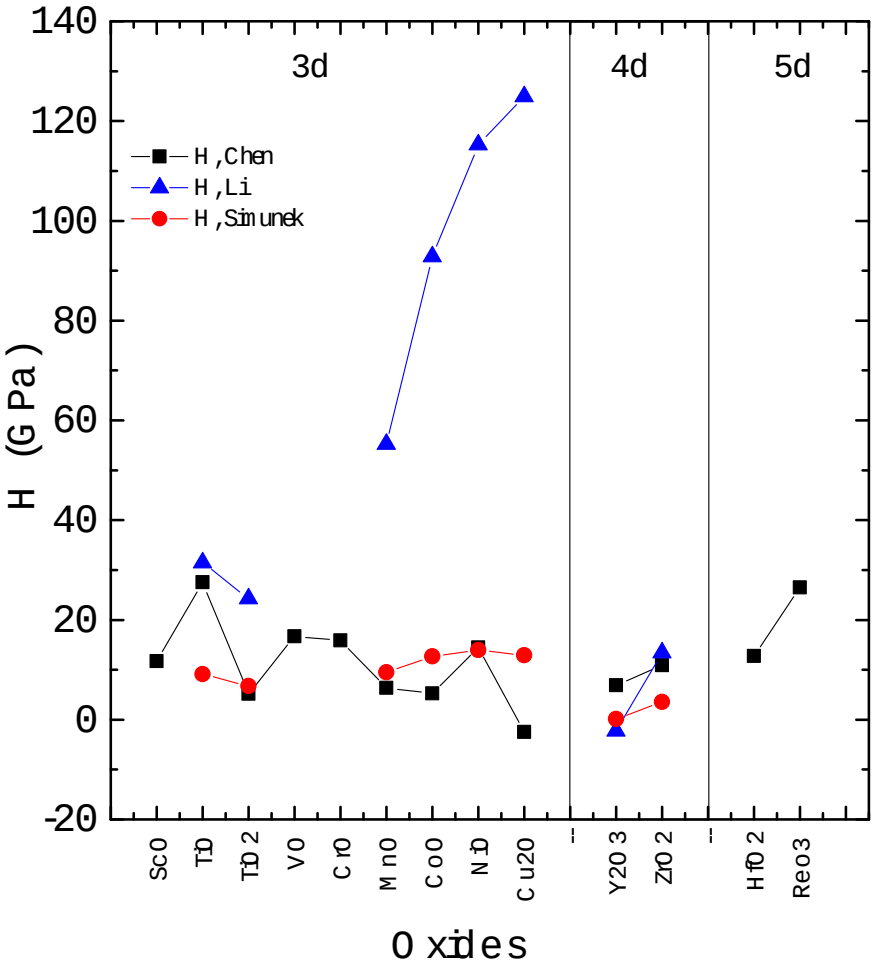

Figure 2.5: Calculated hardness values of transition metal oxides in different structures.

2.5 Evaluation of the investigated methods

In the previous chapters, the calculated values were tabulated, but not yet evaluated. This overdue task will be tackled here.

In Fig 2.6 the calculated hardnesses can be seen versus experimental literature values. Three lines show an ideal agreement of experimental and calculated values, as well as an $\pm$ 10 % offset. This value was chosen, because experimental values in general are suspect of a 10 % measurement inaccuracy . Especially very hard materials are difficult to measure which the controversy around Chung et al. (2007) on the hardness of ReB_2 shows[83].

The values are grouped, so that data points in the same colour are of the same material type. Nitrides seem to follow the ideal line the best. Values are concentrated in the 10 % offset region, which shows a good agreement of model and reality. For diborides and carbides in contrast, this trend cannot be observed. Both of them seem to scatter randomly. For these two material families, no general agreement with the models at hand can be seen. It is also not apparent, if they mainly over- or underestimate the values. This first graph was produced to show possible correlations between material groups and the predictability of their hardness. For diborides and carbides this could not be seen, but for nitrides it seems, that the models agree well with experimental data. Nevertheless further analysis is necessary.

To compare the methods with each other, the diagram was changed, so that one method is shown in one colour, and the different material families are shown in differently shaped data points, which can be seen in fig 2.7. The method by Šimůnek provides some reasonable values, but overestimates some materials vastly. In this representation the good agreement of values computed with the method by Chen can be seen. Only one data point with a very strong missmatch can be seen, RuB_2, with a calculated hardness of 1.4 GPa versus 19.9 in experiments, however no clear reason for this behviour could be found. The other values lie within the error margin or close to it.

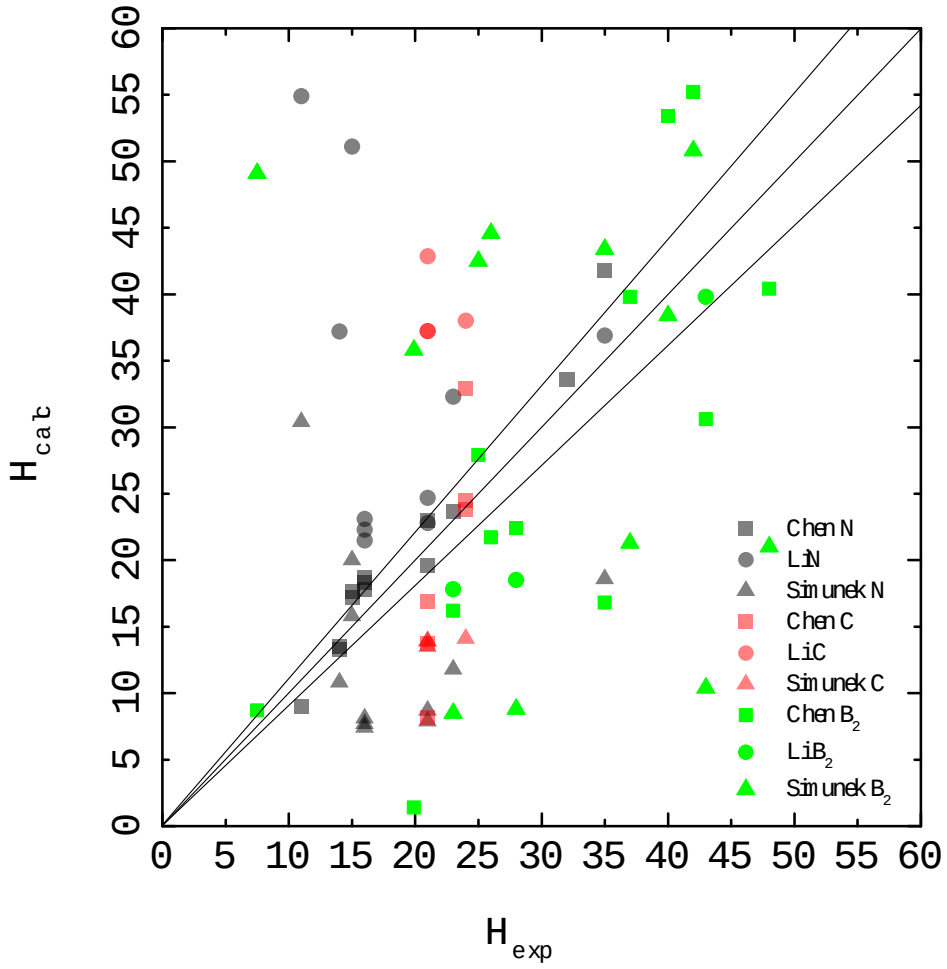

Figure 2.6: The calculated values of hardness versus experimental values, as well as an 10% error bar. Material classes have the same colour, while methods used have the same symbol.

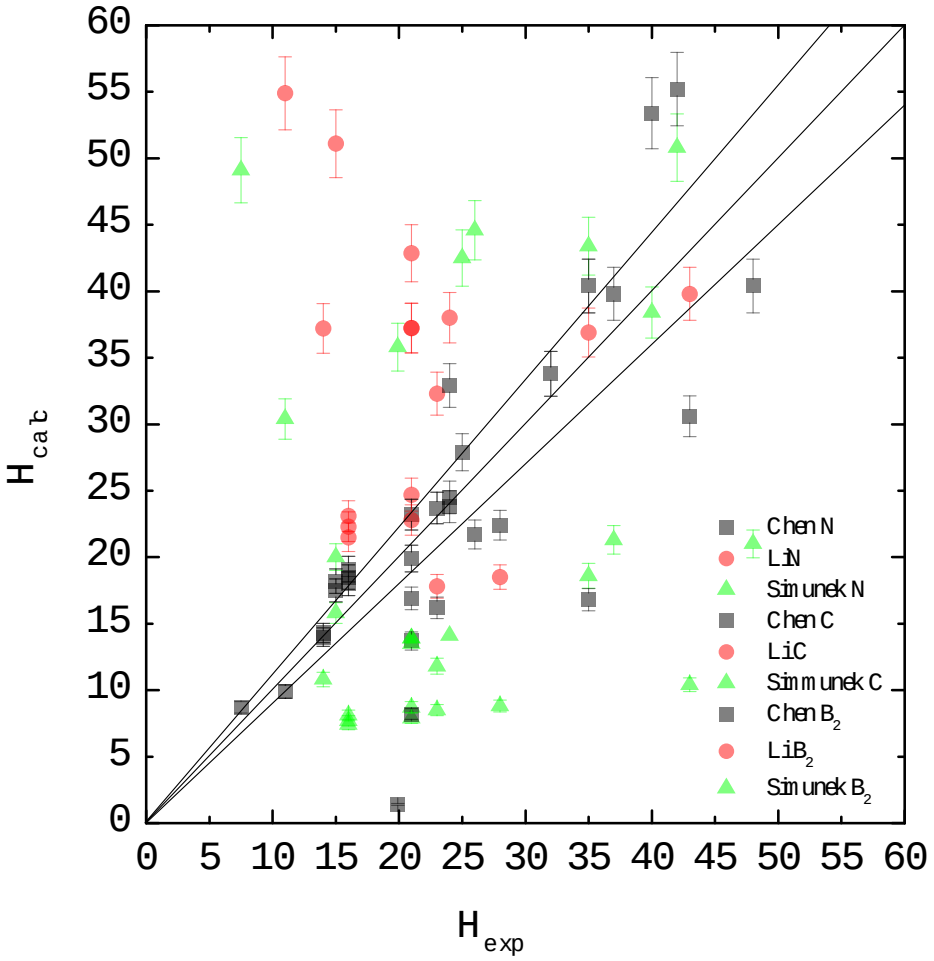

Figure 2.7: The calculated values of hardness versus experimental values. The methods are depicted in green (Šimůnek), red (Li), black(Chen) as well as an 10% error bar.

3 Materials project

Ever since computational power came to be available for research, scientists dreamed of predicting new materials with special properties only by means of workstations and supercomputers. With the development of quantum mechanics, a word first used in a paper in 1924 by Max Born [84], the tools to predict various materials properties came to be available. But only with the advance of computer technology from the 1940s to today, was it possible to apply this theory to a wide range of problems, e.g. in calculating electronic structure, band gap, energy of formation or elastic properties. With the availability of fast internet connections and big data storages, online databases became more and more common.

In this chapter, the online database "Materials Project" will be used, to get access to the elastic constants of transition metal nitrides, oxides, carbides and borides. Firstly, the process of collecting the data via a Python script will be discussed. After that, some properties that were used to evaluate the methods will be compared with values from the online database. Subsequently hardness and fracture toughness will be calculated and plotted and general trends will be discussed. Last but not least, the investigated compounds will be divided according to their elastic behaviour into brittle and ductile.

3.1 Data acquisition

Materials Project provides a Python library, which can be utilised to search for properties of materials. In this work, a Python script was written allowing one to automatically download and format materials properties. The script can be seen in Appendix a. It queries the elastic tensor, the chemical formula, volume of the unit cell and the calculated elastic properties (shear and bulk modulus) of compounds that fulfill certain search parameters, e.g. having one specific element in them and an available elastic tensor. This reduces the amount of possible materials from 86.000 to 13.000, as of January 2019. Since the focus of this thesis is on the ceramic like materials, the number is reduced to 4.700 that contain at least one of the searched for elements (N, C, O, B).

3.2 Comparison of elastic constants

In this section some shear and bulk moduli of transition metal diborides, extracted from materials project and from Moraes et al. [65] will be compared.

First, the shear modulus will be compared, as can be seen in fig 3.1a. The average values agree very well, with MnB_2 being an outlier. The bulk modulus, fig 3.1 b, shows a good agreement of general trends, however the two lines do not agree as well as for the

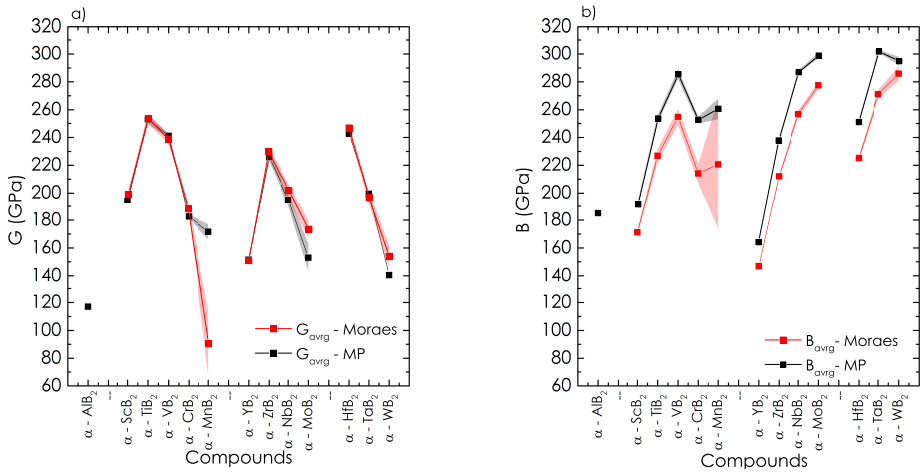

Figure 3.1:
The Voigt-Reuss-Hill (VRH) average shear (a) and bulk (b) modulus of different diborides in α structure calculated by Moraes et al (red) and Materials Project (black) can be seen. The good agreement of some points, as well as the disagreement of others can be easily seen. The dyed areas show upper & lower bounds of elastic constants.

shear modulus. For instance VB_2 has calculated moduli of 255 GPa or 285 GPa, when elastic tensors are taken from Moraes et al. or Materials Project, respectively. This discrepancy between the two datasets stems from differences in the elastic tensors.

Another point, that can be seen, is that upper and lower bound, depicted by the red and black shaded areas in fig 3.1 a and b lie very close to each other.

3.3 Hardness and fracture toughness

In fig 3.2 the calculated hardness and fracture toughness values can be seen. All the values were calculated with the formulas by Chen et al. and Niu et al. [23, 27]. The considered compounds had hardnesses below 100 GPa and fracture toughnesses below 7 MPa$\sqrt{m}$. Some compounds were calculated to have hardnesses well above 100 GPa. These very high hardnesses sound very promising in the search for new superhard materials, however all of such materials have negative shear or bulk moduli. However compounds and composites with negative shear modulus are not stable according to Wang et al. [85] and negative bulk modulus is possible, e.g. due to a volumetric phase transformation in cerium at 117 K. In this work however, this type of materials are neglected, due to the very special conditions they exist in.

The nitrides can be seen in fig 3.2a. The majority of data points lies in the region below $H_v = 20$ GPa and $K_{IC} = 3$ MPa$\sqrt{m}$. Some of the compounds, like cubic BN (215) and BC_2N, agree very well with experimental data [86], and are used in industry and research. These hard phases contain only light elements, which hints to a high degree

of covalent bonds, as reported by e.g. Teter (1998) [51]. TiN, a material widely used in industry, in it's cubic phase ($H_v = 30$ GPa), could in this work be found in another spacegroup (216) with an even higher hardness of $H_v = 45$ GPa. However no literature values about this allotropy could be found.

In Figure 3.2b, compounds containing at least one carbon atom can be seen. Again a high density of points can be seen in the area below $H_v = 20$ GPa and $K_{IC} = 3$ MPa$\sqrt{m}$. Some well known materials, for instance WC agree very well with experimental data by Haines et al. [11]. Also diamond at around $H_v = 100$ GPa and $K_{IC} = 6.5$ MPa$\sqrt{m}$ agrees very well with experimental data by Gao et al. [87]. Other notable results are from Be_2C, which was already investigated by the U.S. department of Energy in 1956, reporting a hardness similar to that of SiC ($H_v = 31$ GPa) [88, 89].

Materials that contain oxygen are shown in fig 3.2c. Again it can be seen, that most of the calculated hardness values lie below 15 GPa and the fracture toughness below 2.5 MPa$\sqrt{m}$. The reason for the high density of points in this graph, lies in one of the aims of Materials Project, finding new electrolytes and contacts for batteries. In this application oxides play a very important role, therefore the amount of them is higher, when compared to the other three compound groups (nitrides, carbides, borides). Perovskites such as $GePbO_3$ are interesting compounds, which are used and researched in Li-Ion battery technology[90]. Others such as $SiSnO_3$, $CaMnO_3$, or $RbAsO_3$ have high hardnesses and low fracture toughnesses. In the hard oxides this group of materials makes out half of the compounds with $H_v > 40$ GPa. Another quite apparent feature of the oxides, is that the harder oxides all have fracture toughnesses below 2 MPa$\sqrt{m}$, while the other systems (N, C, B) have fracture toughnesses 2-3 times higher than that.

The fourth group, shown in fig 3.2d, are the borides. In this figure, some of the already discussed compounds, such as BN, BC_2N and BC_5 can be seen. Most of the boride containing materials can be found in the region below $H_v = 30$ GPa and below $K_{IC} = 4$ MPa$\sqrt{m}$. In the harder and tougher compounds a big group of mostly transition metal diborides can be identified, consisting of : TiB_2, HfB_2, ZrB_2, UB_2, UCo_3B_2. All of those crystallise in space group 191 and have hardnesses above 40 GPa, which makes them superhard. With the exception of UCo_3B_2, they also have fracture toughnesses of above 3 MPa$\sqrt{m}$. Some of these diborides have already been synthesised and are well described in literature, e.g. Deng et al. (1995) [91], Andrievski et al. (1998) [92], Rogl et al. (1983) [93] or Gu et al. (2008) [72].

In conclusion it can be said, that oxides generally have lower fracture toughnesses, when compared to nitrides carbides and borides. A reason for this behaviour might be, that oxygen is the element with the highest electronegativity, therefore it can be assumed, that covalent and ionic bonds are more common than in nitrides, carbides and oxides, which are known to have lower K_{IC} values than compounds with predominantly metallic bond [27]. Due to the same reason, directional (covalent) bonds are stronger, harder materials can be found.

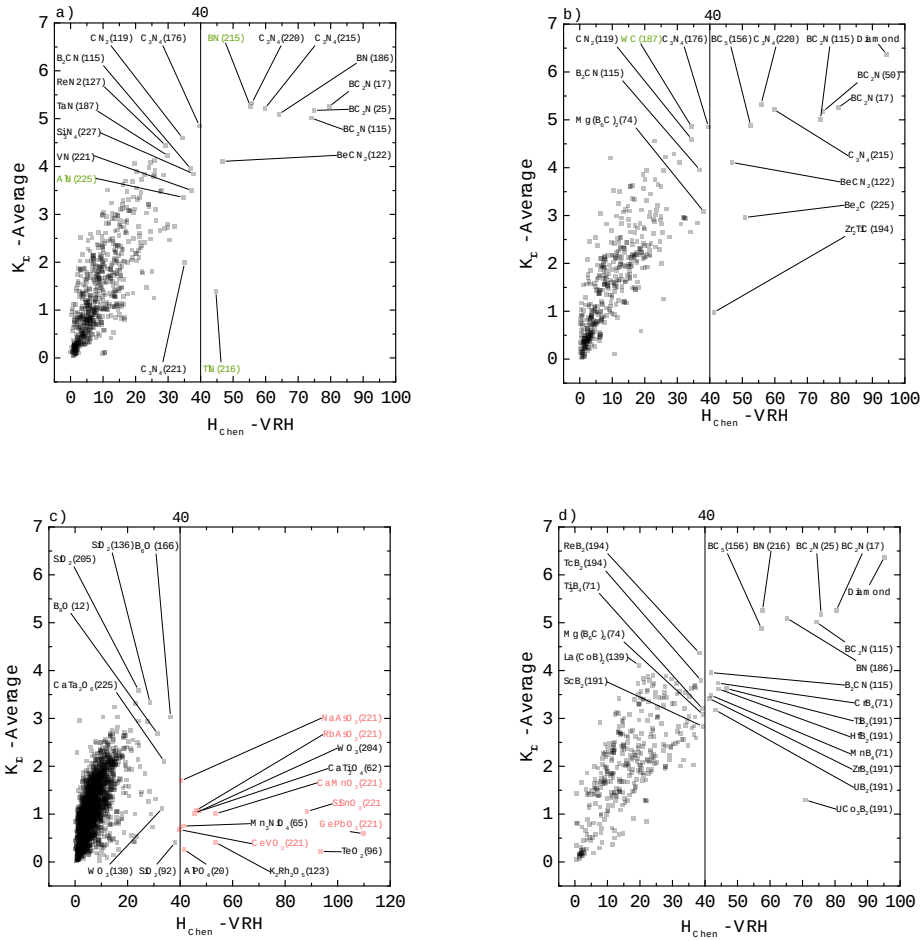

Figure 3.2: Comparison of compounds containing either at least one N (a),C (b),B (c), O(d) with more ore equal than 1 other and less than 3 other elements.

3.4 Ductility

In this section the results of two semi-empirical criteria for ductile behaviour are shown in fig 3.3. The prediction of brittle to elastic answer to tensile stress, is an important one, as for different applications more or less ductile behaviour is preferred. For instance steel used for bridges or other structures, can deform to some extent, to incorporate deflections due to e.g. wind or other environmental influences.

The ductility of nitrides can be seen in fig 3.3a. Very hard materials, like diamond, BC_2N or c-BN can be found on the brittle end of the scale with low Cauchy pressures and high Pugh ratios. Furthermore when comparing hard TiN (25 GPa) with softer materials like NbN (13GPa), CrN (10 GPa) or VN (16 GPa), it is apparent that some of the softer nitrides are more ductile than the harder ones. Another point that can be made, is that the two different criteria are consistent, meaning, that there are very few materials, that are characterised as brittle by one and ductile by the other formula.

In fig 3.3b the carbides can be seen. In the region of very low Cauchy pressures, below -200 GPa the same compounds as in fig 3.3a, except for BC_5 are shown. In this region, where high brittleness is prevalent, most of the superhard materials can be found. A second interesting compound is Zr_2TlC, which was calculated to be superhard at 40 GPa and has been discussed e.g. by Bouhemadou et al. (2009) and synthesised by Jeitschko et al. (1964) [94, 95], however no experimental hardness values were reported. The ductile area with positive Cauchy pressure and Pugh ratios below 0.57 shows some interesting materials as well. VC, NbC and TaC were discussed by Li et al. [96] as well and agree reasonably well with experimental data, while RuC (225), in this plot calculated to be very ductile at a Cauchy pressure over 200 and a Pugh ratio below 0.15, was calculated to be hard at 25 GPa [96].

The investigated oxides can be seen in fig 3.3c. A point that was made in chapter 3.3 was, that a majority of the hard oxides are perovskites in spacegroup 221. It can be seen, that this class of materials can be very ductile as well, e.g. $VCdO_3$, $RbFeO_3$ or $AlCoO_3$. These three compounds have hardnesses of 1.6 GPa, 1.5 GPa and 1 GPa, saying that they are very soft, as well as having high Poission's ratios close to 0.5, which makes them behave rubber like. For those three compounds no literature values of any kind could be found. PbO_2, a material which is used as an anode material in lead batteries, was calculated to be the dioxide with the highest ductility, at a Cauchy pressure of 190 and a Pugh ratio of 0.16. On the other end of the spectrum, TeO_2 is calculated to be one of the most brittle materials, which is used as glass and glass base compound [97]. A material that appears to be very brittle is $RbCdO_3$, however when looking at the shear modulus and bulk modulus (4.5 and 1 GPa respectively), it follows, that the Poisson's ratio is negative, meaning, that when stretched this material becomes thicker perpendicular to the stretch direction. B_6O, being on the more brittle side, a material synthesised by e.g. Hubert et al. [98], experimentally shown by He et al. [99] to be superhard at 45 GPa, is an compound with short directional bonds.

The last group shown here in fig 3.3d is the group of borides. In this graph, two relative ductile monoborides are shown. TcB was studied by Li et al. (2010), however these values are in no good agreement with the values used here [100]. In 1960 Aronsson

et al. reported that PtB crystallises in spacegroup 194, which is also shown here to be very ductile [101].In the Region below 200 GPa Cauchy pressure, the same compounds can be found as in the figures discussed above. Four transition metal diborides are depicted here, where HfB_2, TiB_2 and UB_2 are shown in spacegroup 191 and ReB_2 in W_2B_{5-x} structure, which was reported e.g. by Moraes et al. to be the preferred structures [65]. UCo_3B_2 is a material, which was expected to be a strong permanent magnet, by Sterer et al. [102]. The reported X-ray powder diffraction patterns show a stable phase of the compound in spacegroup 191 [102]. Be_4B was reported to be stable in space group 129 [103]. B_2CN is shown in three different structures, this was done, to show the difference in ductile to brittle transition depending on the spacegroup of the compound. Lastly, LiBeB, a compound that is of interest for cosmology because of it's formation during supernovae, was reported to be theoretically stable down to pressures of 15 GPa by Hermann et al. (2012) [104].

To sum up the four plots, it can be said, that the oxides, when compared to the other three, have much higher Pugh ratios but higher Cauchy pressures in the brittle area with Cauchy pressures below 0 and Pugh ratios above 0.57.

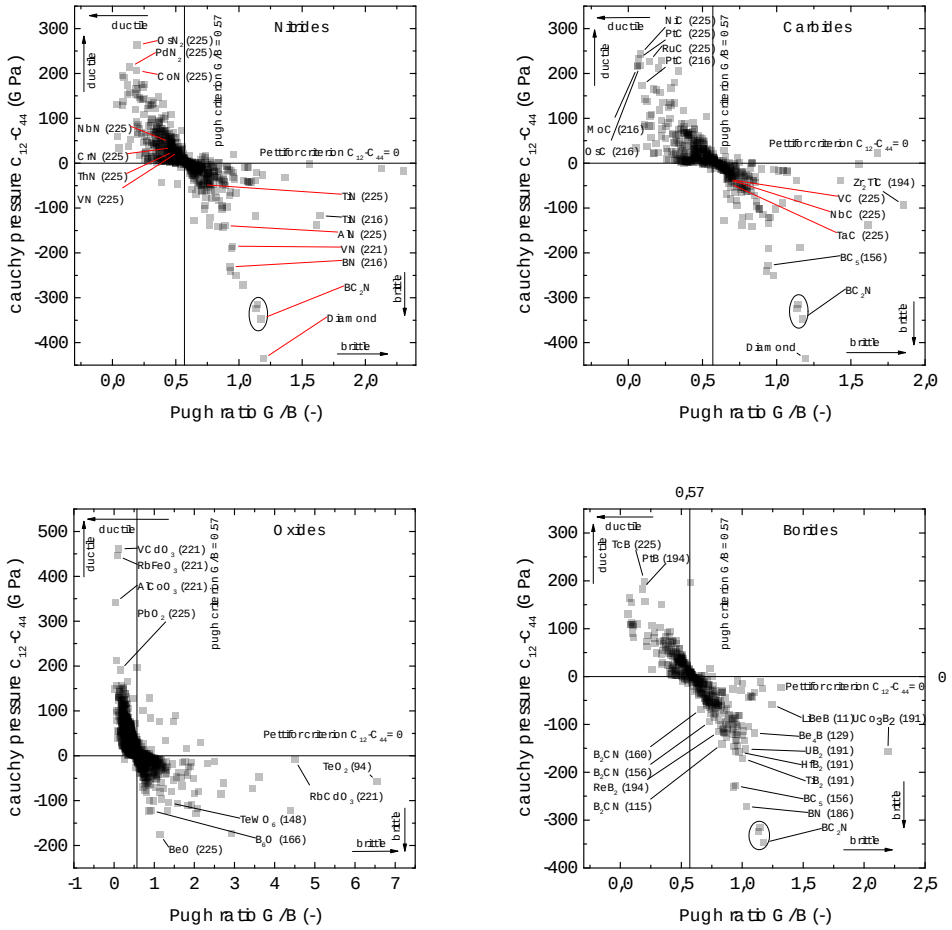

Figure 3.3: Comparison of compounds in terms of their ductile to brittle behaviour with N (a),C (b),O (c),B (d) .

4 Ternary transition metal compounds

So far mainly binary and some ternary compounds, when their elastic constants were readily available, were investigated. However most of the binary systems are already well researched, therefore ternary or quaternary transition metal compounds are of great interest. In this chapter the hardness of ternary compounds with the formula ABX (A,B=transition metal, X=N, C, B or O) will be calculated.

The best solution to get reliable predictions for ternary compounds, would be to calculate elastic constants via DFT of the compound of interest. This method should produce the most trustworthy results, and therefore the most accurate predictions. However it is quite time-consuming, as calculations take time and knowledge about the elemental system on hand, therefore a quicker solution would be to take the binary systems, with available elastic constants, and calculate the hardness gain/loss expected to occur when they are mixed.

For all the calculated values in this chapter, elastic constants from Materials Project were used. The intrinsic hardening mechanisms were already discussed in the introduction as well as the available hardness models.

In a first step, the method was evaluated, by applying it to two well known compounds, $Ti_{(1-x)}Al_xN$ and $Cr_{(1-x)}Al_xN$. The resulting H_v values were compared with experimental hardnesses as well as with hardnesses calculated with elastic constants from the ternary compound.

In fig 4.1a the relatively low strengthening potential of $Ti_{(1-x)}Al_xN$ can be seen. This behaviour results from the relatively low lattice mismatch of AlN and TiN. It can be seen, that all data follow a general trend, where at higher Al concentrations, the hardness increases. The calculated values, with solid solution strengthening, agree very well with experimental values by Santana et al. [105]. While experimental values by Kutschej and Chen [106, 107], agree better with the hardness values calculated with linearly interpolated elastic constants. The hardness values based on DFT calculated elastic constants by Tasnadi et al. [108], agree well with experimental values by Kimura et al. [109]. On the other side in fig 4.1b, the second well observed system (CrAlN) is shown. Here elastic constants for the ternary systems by Zhou et al. were used [35], it can be seen, that for higher AlN contents, the hardness values agree very well. The experimental values by Sanchez-Lopez et al. [110], are higher than the calculated hardness values. This behaviour could stem from the fact, that thin films are generally harder than bulk materials, which are calculated by DFT methods.

In fig 4.2a the strengthening of the diboride of hafnium and zirconium is presented. It shows already quite a big strength increase at very low fractions of Zr in the hafnium diboride lattice, but also the other way around. According to the model, the highest strength increase occurs at a 50:50 mixture of Zr and Hf.

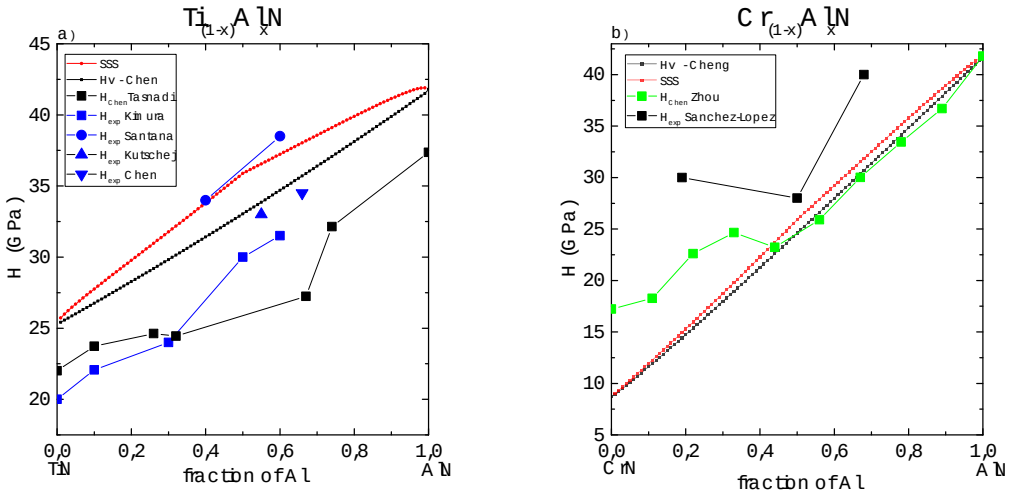

Figure 4.1: Hardness of the ternary systems TiAlN (a) and CrAlN (b) with linear interpolated elastic constants vs hardness with a solid solution strengthening factor. As well as experimental data and hardness values calculated from elastic constants for the ternary system.

In the system titanium zirconium carbide, depicted in fig 4.2b, we can see a very high hardness increase. This might stem from the high lattice mismatch of 0.388 Å. The highest strengthening potential can be seen when both binary compounds are mixed in an equal ratio. The maximum strengthening potential is 5 GPa, the resulting hardness is $H_v = 28$ GPa.

Fig 4.2c shows the system $CrWB_2$. The diboride of tungsten and chromium, show very different hardness values, when compared to each other. α CrB_2 has a hardness of 26 GPa, while α WB_2 shows a hardness of 14 GPa. The two compounds have a low latticemismatch of 0.063 Å, which results in a relatively low strengthening potential of roughly 1.5 GPa, when comparing the linear interpolated hardness values (black line) with the ones with an added strengthening factor (red line).

The higher strengthening potential of $TiCrB_2$, depicted in fig 4.2d, when compared to $CrWB_2$ can partially be attributed to the higher latticemismatch of 0.076 Å.

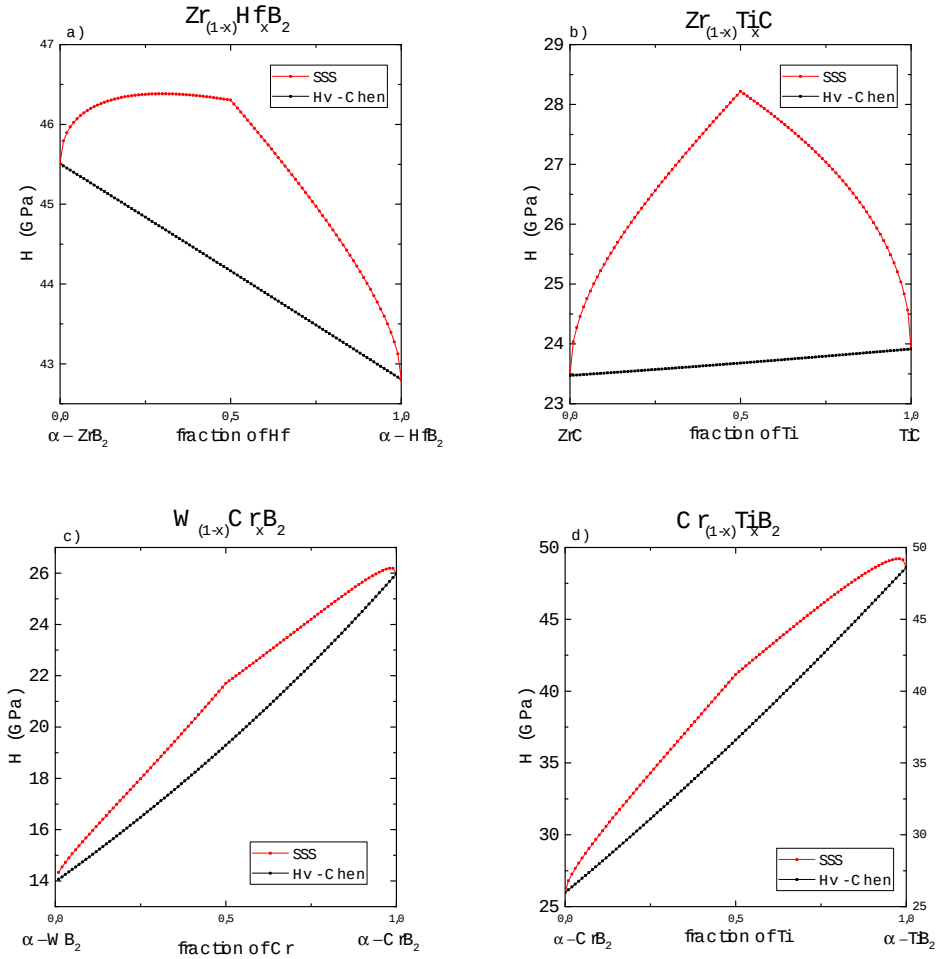

Figure 4.2: Solid solution strengthening effect in the systems $Hf_xZr_{(1-x)}B_2$ (a), $Ti_xZr_{(1-x)}C$ (b), $Cr_xW_{(1-x)}B_2$ (c) and $Ti_xCr_{(1-x)}B_2$ (d). The red line shows the hardness with an added solid solution strengthening factor, while the black line shows the hardness values calculated with the linearly interpolated elastic constants.

4.1 Experimental

One binary ZrB_2 and three ternary borides within the materials system Zr-Hf-B_2 were produced in the form of coatings deposited using a modified magnetron sputtering system - Leybold Heraeus Z400- in mixed Ar and N_2 glow discharges (both gases with purity above 99.999%). ZrB_2 (Ø75 mm) was utilised as the main target, while HfB_2 target was broken into small fragments and 4, 8 or 12 fragments were uniformly distributed on the racetrack of Zr target, in order to vary the metal fraction within the Zr-Hf-B_2 coatings. Both targets, ZrB_2 and HfB_2, with a purity of 99.95 mol.% were produced by means of powder metallurgy by PLANSEE SE. All depositions were prepared using the constant target current (DC) of 0.5 A, bias voltage of -50V, and substrate temperature of 350 ± 20 °C. Prior to every deposition process, the chamber was evacuated to a high vacuum of $p_{\text{base}} \leq 3.2 \cdot 10 - 5mbar$. The total pressure, p_T, of 0.35 Pa and N2-to-total-pressure ratio, p_{N2}/p_T, of 0.32 were kept constant for all deposition processes. The substrates made of single-crystal silicon and sapphire as well as polycrystalline austenite steel were ultrasonically pre-cleaned in acetone and alcohol (for 5 min in each) and r.f. plasma etched within the deposition chamber using an Ar flow rate of 60 sccm and a substrate potential of 150 V. After each deposition process, the substrates were cooled down to at least 90-100 °C before venting the deposition chamber, in order to minimise the surface chemistry alterations [111].

Phase analysis was carried out by means of X-ray diffraction (XRD) in Bragg-Brentano geometry using monochromised CuKα radiation (λ=1.5406 Å). The chemical composition of our coating was evaluated based on energy dispersive X-ray spectroscopy (EDS), which was calibrated using SECS light-element calibration standard CaB_6 (Ardennes Analytique SPRL). Indentation hardness, H, and modulus, E, of the coatings were obtained by evaluating the load–displacement curves of nanoindentation tests (Berkovich diamond tip and load range of 3 - 45 mN) after Oliver and Pharr [3], described in detail elsewhere [112–115].

4.1.1 Results & discussion

The XRD measurements of the samples are shown in fig 4.3. Sharp peaks can be seen, therefore all of them are crystalline. When comparing the peak at 92° between the four different thin films, ZrB_2 (LM01) and the two Zr−Hf−B (LM03 and LM04) phases on top show symmetrical peaks, while the second peak from the bottom (LM02) show some peak broadening. This behaviour might stem from the use of -50V bias voltage, which was only applied for this sample. Similar effects can be seen for the peaks at 42° and 64°. From this distinctive feature it can be deduced, that sample LM02 contains more than one phase with different lattice parameters. Samples LM01, LM03 and LM04 show behaviour that suggests single-phased TMB_2 solid solutions, except for sample LM01 which only consists of ZrB_2. Similar results can be seen in Mayrhofer et al. (2018) [116]. The measurements were carried out on Al_2O_3 substrates, because in two of the experiments the silicon wafers broke during the experiment possibly due to high stresses. The exact time, when the Si substrate broke is not known, but it is possible, that Si

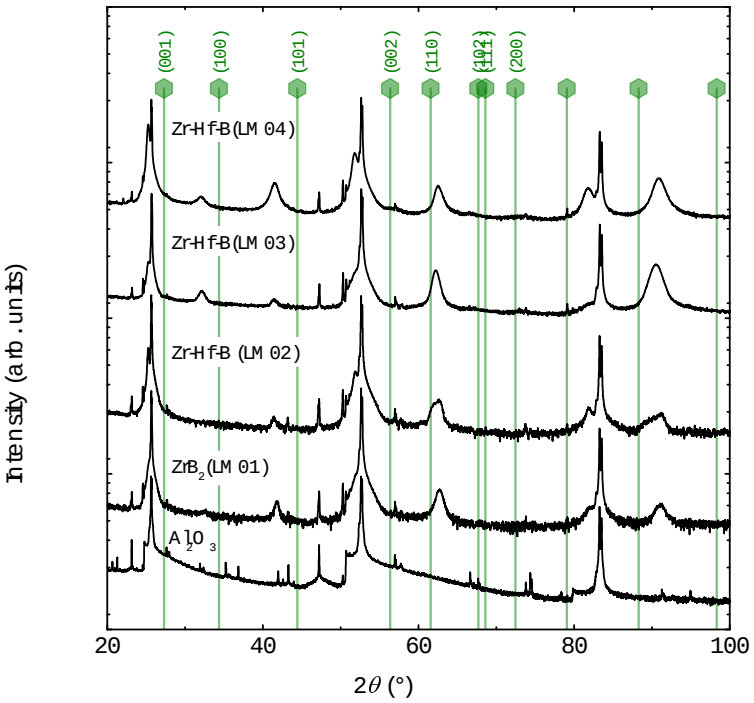

Figure 4.3: XRD diffraction pattern of four samples on Al_2O_3 substrates.

shards were present on the target during the sputtering process. Si contamination is possible in samples LM03 and LM04.

To detect possible Si contamination EDS measurements were conducted. The results can be seen in table 4.1. However due to the Si Kα and Kβ peaks at 1.739 keV and 1.837 keV being in close proximity to the Hf Mα and Mβ peaks at 1.644 keV and 1.700 keV it was not possible to detect any silicon. Even when the software was only given the choice to detect Si, it could not detect any, due to the peak overlap. Sample LM01 was sputtered without any Hf cubes on the racetrack, but the chemical analysis suggests 1.9 at.% Hf. This might stem from impurities in the target, Hf and Zr are hard to separate as reported by Xu et al. [117]. In the other samples, the Hf content increases continuously, from 24.5 at.% to 58.1 at.% with the amount of Hf fragments in the racetrack. The boron content decreases steadily from 77.5 at.% to 71.2 at.%, bringing it closer to the equilibrium ratio of 66.66 at.% (shown in red), which can be seen in fig 4.4, meaning that all four thin films are over-stoichiometric. This behaviour could stem from different sources:

- Boron interstitials
- Metallic vacancies
- Boron atoms on anti sites

Table 4.1: Chemical composition and hardnesses of the sputtered diborides.

	chemical composition at%			fraction of %		hardness GPa	E modulus GPa
	B	Zr	Hf	Zr/(Hf+Zr)	Hf/(Hf+Zr)		
LM01	77.5	22.1	0.4	98.2	1.9	46.3±2.3	496±19
LM02	73.9	19.6	6.5	75.5	24.5	44.8±3.2	476±16
LM03	71.3	16.3	12.5	57.4	42.6	48.4±1.8	505±26
LM04	71.2	11.8	17.0	42.0	58.1	49.3±4.0	529±23

All of the above push stoichiometry to higher boron contents.

The hardness reported in table 4.1 and fig 4.5, shows the lowest value for sample LM02, which was the only one sputtered with -50V bias voltage. Here it should be mentioned, that in samples LM01 and LM02 the two Si wafers that were sputtered did not break, while for samples LM03 and LM04 they broke at some point during the experiment. It is possible, that due to internal stresses, the hardness in sample LM02 is lower, while for the latter two samples, the silicon had an positive effect on internal stress and hardness. Sample LM01 shows good agreement to literature values (this work 46.3 ±2.3 GPa, Mayrhofer et al.(2018) 44.8 ±2.3 GPa [116]). When compared to the calculated hardness value of 45.8GPa, the good predictive power of this method is apparent. As the model uses ideal crystals and doesn't account for grain size underestimation can be assumed, which is the case. For the first sample LM01 the experimental values show ΔH of 1 %. The second one, LM02, lies 3.5 % below the calculated hardness, however it is the sample with inconclusive XRD pattern. For samples LM03 and LM04 the difference of calculated to experimental hardness is 4.5 % and 7.4 % respectively. With nature of this method in mind, it can be said, that for $Zr_{(1-x)}Hf_xB_2$ the prediction was quite promising, and the experiments exceeded those predictions.

The aim of this work was to find new hard and tough phases, and ideally find a way to quickly do so. This was achieved by finding different ways to calculate hardness and fracture toughness, evaluating these methods and applying the winner (Chen's formula as well as Niu's formula) to a big dataset (Materials Project). Finally a way to calculate hardness of ternary transition metal compounds was used, to predict these type of materials with ease and one exemplary compound was synthesised and tested to its predictions. This comparison of calculations and experiment was successful, however further research is necessary to thoroughly evaluate this method.

In general it can be said, that, when used correctly, this method is useful to quickly find estimates of hardness and fracture toughness for unknown materials. One should keep in mind, that the formulas simplify material behaviour, e.g. not taking grain size into consideration or assume ideal crystals, and that they are only valid for brittle materials. Therefore already in early stages of material selection, these should be remembered, not to choose some with e.g. negative shear modulus, which are normally elastic rubbers and per definition not hard. When those points are taken into account however, it is fairly easy to cover many different material combinations in little time.

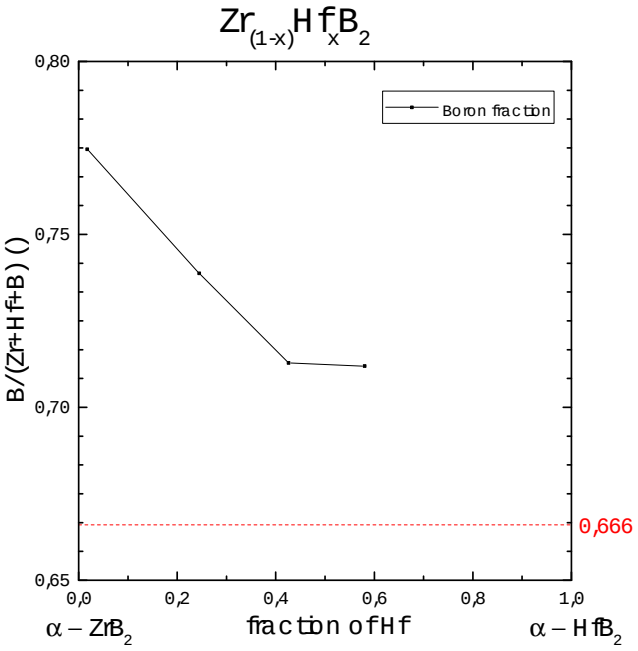

Figure 4.4: Boron content as a function of Hf fraction.

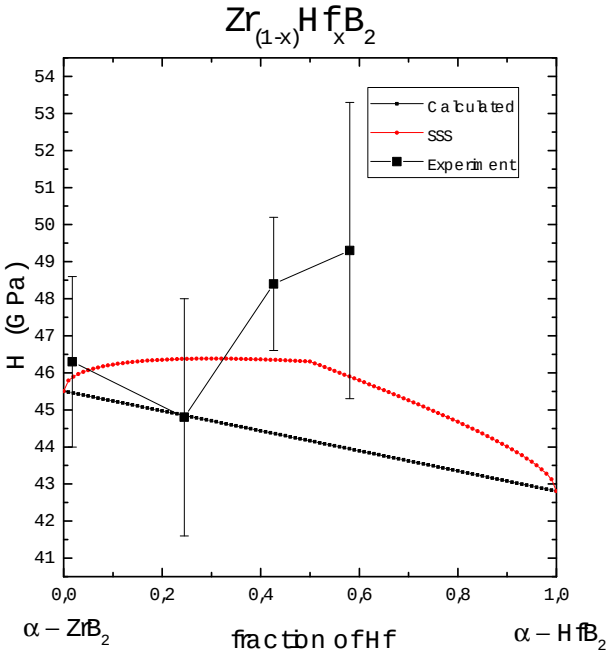

Figure 4.5: The calculated hardness versus the experimental values.

5 Résumé

Finding new hard and tough materials is a complicated process, described in this thesis. The steps taken in this work will be briefly summarised in this chapter, after that the conclusions will be discussed and lastly the question why this work is important will be answered and some questions for further research will be posted.

In the first chapter, the question why hard and tough materials are needed and what the main factors in composing hard and tough materials are, were answered. Furthermore methods to calculate these properties from literature were introduced and compiled in an comprehensive overview. With this knowledge, the formulas were taken to the test in chapter two, where the hardness and fracture toughness of transition metal nitrides, carbides, borides and oxides with properties taken from literature were calculated, compared and the different methods were evaluated. While all formulas show good results for specific materials, the two (H_v and K_{IC}) best suited for the application in ceramic-like materials were then applied in chapter 3, to calculate hardness and fracture toughness of 4.700 compounds available in the database "Materials Project". Some of the calculated values were compared with data used to evaluate the formulas, general trends were discussed. In chapter four ternary transition metal compounds were investigated, by applying a method, that uses data from the underlying binary compounds (which is readily available), to calculate the hardness of the ternary compound (solid solution strengthening). Finally one of the ternary compounds was synthesised using PVD, and the agreement of experimental to calculated hardness was shown.

The question that needs to be answered next is, what can we learn from these findings. Firstly some general remarks about the methods. As stated before, all formulas have their applications, where they provide excellent results. However for ceramic-like hard materials the formula proposed by Chen et al. and Niu et al. predict hardness and fracture toughness, respectively, with the highest accuracy. showed to be the most useful. Secondly knowledge about bond type can help provide more accurate predictions, by using the most suitable model, however in transition metal compounds this is a complicated undertaking.

With these conclusions at hand, what are some questions that could not be answered in this work. The most important one is probably the characterisation of bond types. In this work only intrinsic properties of ideal crystals were discussed, however in reality crystal lattices have defects and extrinsic strengthening mechanisms like the Hell-Petch effect are applied, which are needed to be account for in order to improve the prediction accuracy for real materials..

On a final note, the importance of high quality experimental data should be mentioned. For future works a database of experimental H and K_{IC} values could make a difference in the time needed to evaluate methods, but also the quality of the evaluation.

Appendices

```
from csv import reader as csv_reader
from math import cos, sqrt, pi
from pymatgen.ext.matproj import MPRester
from pymatgen.core import Element
from os.path import exists
from csv import writer
import pickle
TEMP_FILE = 'mp.pickle'
API_KEY = "neJopyc4HJdrSQLmoB"
EXPORT_FILE = 'ORIGIN_DATA.csv'
def query_materials_project(query, properties):
    with MPRester(API_KEY) as materials_project:
        return materials_project.query(query, properties)
def get_materials_project_data():
    #Umschreiben fuer Nitride oder Oxyde
    query = {'elements': {'$in': ['C']},
             'nelements': {'$gte': 1, '$lte': 3},
             'elasticity': {'$exists': True}
             }
    properties = ['elasticity', 'pretty_formula', 'structure', '
       spacegroup','unit_cell_formula']
    if exists(TEMP_FILE):
        with open(TEMP_FILE, 'rb') as src:
            mp_data = pickle.loads(src.read())
    else:
        mp_data = query_materials_project(query, properties)
        with open(TEMP_FILE, 'wb') as dst:
            dst.write(pickle.dumps(mp_data))
    return transform_materials_project_data(mp_data)
def transform_materials_project_data(d):
    result = {}
    for entry in d:
        key = (entry['pretty_formula'], int(entry['spacegroup'][
           'number']))
        kv = entry['elasticity']['K_Voigt']
        gv = entry['elasticity']['G_Voigt']
        kr =  entry['elasticity']['K_Reuss']
        gr =  entry['elasticity']['G_Reuss']
        nu_v = (3.0 * kv - 2.0 * gv) / (2.0 * (3.0 * kv + gv))
        nu_r = (3.0 * kr - 2.0 * gr) / (0.00001+(2.0 * (3.0 * kr
            + gr)))
        elasticity = {
            'tensor': entry['elasticity']['elastic_tensor'],
            'G_Voigt': gv,
```

```
                'K_Voigt': kv,
                'G_Reuss': gr,
                'K_Reuss': kr,
                'nu_r': nu_r,
                'nu_v': nu_v
            }
            l = entry['structure'].lattice
            lattice = (l.a, l.b, l.c, l.alpha, l.beta, l.gamma)
            result[key] = {
                'elasticity': elasticity,
                'lattice': lattice,
                'num_sites': len(entry['structure'].sites)
            }
    return result
def unictcell (d):
    unitcell = ['unit_cell_formula']
    print (unitcell)
def get_bulk_and_shear_modulus(d, method='v'):
    method = method.lower()[0]
    if not method in 'rv':
        raise ValueError('␣method␣must␣be␣either␣r␣or␣v')
    method = 'Voigt' if method == 'v' else 'Reuss'
    b = d['elasticity']['K_{0}'.format(method)]
    g = d['elasticity']['G_{0}'.format(method)]
    return (b,g)
def hardness_chen(d, method='v'):
    b, g = get_bulk_and_shear_modulus(d, method=method)
    try:
        h =  float(0.92 * (g/b)**1.137 * g**0.708)
    except Exception:
        h = float('nan')
    return h
def unit_cell_volume(lattice):
    a, b, c, alpha , beta, gamma = lattice
    alpha , beta, gamma = (e * pi/180 for e in [alpha, beta,
       gamma])
    volume =  a * b * c * sqrt(1 - cos(alpha)**2 - cos(beta)**2
       - cos(gamma)**2 + 2 * cos(alpha)*cos(beta)*cos(gamma))
    return float(volume)
def fracture_toughness_niu(d, method='v'):
    b, g = get_bulk_and_shear_modulus(d, method=method)
    V0 = unit_cell_volume(d['lattice'])/d['num_sites']
    try:
        kic = float((10**(-30)*V0)**(1.0 / 6.0) * g*1000 * sqrt
```

```
            ((1000*b) /(1000* g)))
    except Exception:
        kic = float('nan')
    return kic
def parse_compound_string(compound, spg, ignore=['B']):
    elements = []
    for i, character in enumerate(compound):
        if i == 0:
            if not character.isupper():
                raise ValueError('Invalid compound')
        if character.isupper():
            if i < len(compound) -1:
                if compound[i+1].isupper():
                    current_element = character
                elif compound[i+1].islower():
                    current_element = character+compound[i+1]
                else:
                    current_element = character
            else:
                #Letzes symbol is ein grossbuchstabe
                current_element = character
        else:
            continue
        if current_element not in elements and current_element
           not in ignore:
            elements.append(current_element)
    elements = [(el, Element(el).number) for el in elements]
    elements = list(sorted(elements, key= lambda t: t[1]))
    return ((compound, spg), elements)
def write_csv(filename, keys, data):
    first_row = ['Compound',
                 'Spacegroup',
                 'K_Voigt',
                 'G_Voigt',
                 'K_Reuss',
                 'G_Reuss',
                 'nu_r',
                 'nu_v',
                 'H_Chen_Reuss',
                 'H_Chen_Voigt',
                 'K_IC_Niu_Reuss',
                 'K_IC_Niu_Voigt'
                 ]
    with open(filename, 'w') as export_csv:
```

```
        csv_writer = writer(export_csv)
        csv_writer.writerow(first_row)
        for key in keys:
            compound, spg = key
            d = data[key]
            row = [
                compound,
                spg,
                d['elasticity']['K_Voigt'],
                d['elasticity']['G_Voigt'],
                d['elasticity']['K_Reuss'],
                d['elasticity']['G_Reuss'],
                d['elasticity']['nu_r'],
                d['elasticity']['nu_v'],
                hardness_chen(d, method='r'),
                hardness_chen(d, method='v'),
                fracture_toughness_niu(d, method='r'),
                fracture_toughness_niu(d, method='v')

            ]
            if 'nan' in [str(r) for r in row]:
                print(key)

                #Rausschmeissen
                #continue
            csv_writer.writerow(row)

#
    ##########################################################################

def g_effective(d):
    return (float(d['C11']) + float(d['C13']) - 2 * float(d['C13
        ']) - float(d['C66'])) / 3.0
elastic_properties = {
    'K_Voigt': lambda d: (2 * (float(d['C11']) + float(d['C12'])
        ) + 4 * float(d['C13']) + float(d['C33'])) / 9.0,
    'G_Voigt': lambda d: (g_effective(d) + 2 * float(d['C44']) +
         2 * float(d['C66'])) / 5.0,
    'G_Reuss': lambda d: 1.0 / ((1.0 / g_effective(d) + 2.0 /
        float(d['C44']) + 2.0 / float(d['C66'])) * 1.0 / 5.0),
    'K_Reuss': lambda d: float(d['C13']) + 1.0/(1.0/(float(d['
        C11']) - float(d['C66']) - float(d['C13'])) + 1.0/(float
        (d['C33']) - float(d['C13'])))
}
```

```
def transform_csv_entry(data_dictionary):
    compound_name = data_dictionary['Compounds']
    d = data_dictionary
    crumbs = compound_name.split('_')
    compound_name = crumbs[0]
    # Extract spacegroup
    spacegroup = 191 if crumbs[1] == 'a' else (194 if crumbs[1]
       == 'w' else float('nan'))
    key = (compound_name, spacegroup)
    #Extract lattice
    lattice = (float(d['a']), float(d['a']), float(d['c']),
       90.0, 90.0, 120.0)
    #Assemble elaticity tensor for hexagonal structures
    tensor = [
        [float(d['C11']), float(d['C12']), float(d['C13']), 0.0,
            0.0, 0.0],
        [float(d['C12']), float(d['C11']), float(d['C13']), 0.0,
            0.0, 0.0],
        [float(d['C13']), float(d['C13']), float(d['C33']), 0.0,
            0.0, 0.0],
        [0.0, 0.0, 0.0, float(d['C44']), 0.0, 0.0],
        [0.0, 0.0, 0.0, 0.0, float(d['C44']), 0.0],
        [0.0, 0.0, 0.0, 0.0, 0.0, float(d['C66'])],
    ]
    kv = elastic_properties['K_Voigt'](d)
    gv = elastic_properties['G_Voigt'](d)
    gr = elastic_properties['G_Reuss'](d)
    kr = elastic_properties['K_Reuss'](d)
    nu_v = (3.0*kv - 2.0*gv)/(2.0*(3.0*kv + gv))
    nu_r = (3.0*kr - 2.0*gr)/(2.0*(3.0*kr + gr))
    covalent_radii = [float(d['Rm']), float(d['Rn'])]
    data = { 'elasticity': {
            'tensor': tensor,
            'G_Voigt': gv,
            'K_Voigt': kv,
            'G_Reuss': gr,
            'K_Reuss': kr,
            'nu_r': nu_r,
            'nu_v': nu_v
        },
        'covalent_radii': covalent_radii,
        'lattice': lattice
    }
    #Parameter unpacking
```

```
    return (key, data)
def parse_origin_data(filename):
    with open(filename, 'r') as csv_file:
        reader = csv_reader(csv_file)
        #Takes the first row from the CSV file
        first_fow = next(reader)
        #Skip second row
        next(reader)
        fields_index_mapping = {field_name: index for index,
            field_name in enumerate(first_fow)}
        index_field_mapping = {v: k for k,v in
            fields_index_mapping.items()}
        result = {}
        for row in reader:
            if len(row) == 0:
                continue
            #Skip row if no compound field is given
            if row[fields_index_mapping['Compounds']] == '':
                continue
            entry = {index_field_mapping[index]: field for index
                , field in enumerate(row)}
            key, data =  transform_csv_entry(entry)
            result[key] = data
        return result
if __name__ == '__main__':
    #data = parse_origin_data('binary_borides.csv')
    mp_data = get_materials_project_data()
    #K = key, V = value
    #h_chen_voigt = [(key, round(hardness_chen(value, method='
        voigt'))) for key,value in data.items() ]
    #h_chen_reuss = [(key, round(hardness_chen(value, method='
        reuss'))) for key,value in data.items() ]
    #Sort data by elements
    #sorted_origin_data = list(sorted([parse_compound_string(
        compound, spg) for compound, spg in data.keys()], key=
        lambda t: t[1][0][1]))
    sorted_mp_data = list(sorted([parse_compound_string(compound
        , spg) for compound, spg in mp_data.keys()], key=lambda
        t: t[1][0][1]))
    #sorted_origin_keys = list(map(lambda t: t[0],
        sorted_origin_data))
    sorted_mp_keys = list(map(lambda t: t[0], sorted_mp_data))
    #write_csv('ORIGIN_DATA.csv', sorted_origin_keys, data)
    write_csv('MP_DATA.csv', sorted_mp_keys, mp_data)
```

Bibliography

[1] David G. Rethwisch William D. Callister. *Materialwissenschaften und Werkstofftechnik*. Wiley VCH Verlag GmbH, 21st Nov. 2012. ISBN: 3527330070. URL: https://www.ebook.de/de/product/18549459/william_d_callister_david_g_rethwisch_materialwissenschaften_und_werkstofftechnik.html.

[2] David Richfield. *Stress v strain A36 2*. 2009. URL: https://commons.wikimedia.org/wiki/File:Stress_v_strain_A36_2.svg#metadata.

[3] W.C. Oliver and G.M. Pharr. 'An improved technique for determining hardness and elastic modulus using load and displacement sensing indentation experiments'. In: *Journal of Materials Research* 7.06 (June 1992), pp. 1564–1583. DOI: 10.1557/jmr.1992.1564.

[4] Terry L. Meek and Leah D. Garner. 'Electronegativity and the Bond Triangle'. In: *Journal of Chemical Education* 82.2 (Feb. 2005), p. 325. DOI: 10.1021/ed082p325.

[5] Gordon Sproul. 'Electronegativity and Bond Type: Predicting Bond Type'. In: *Journal of Chemical Education* 78.3 (Mar. 2001), p. 387. DOI: 10.1021/ed078p387.

[6] Gordon D. Sproul. 'Electronegativity and bond type: I. Tripartate separation'. In: *Journal of Chemical Education* 70.7 (July 1993), p. 531. DOI: 10.1021/ed070p531.

[7] Gordon Sproul. 'Electronegativity and Bond Type. 2. Evaluation of Electronegativity Scales'. In: *The Journal of Physical Chemistry* 98.27 (July 1994), pp. 6699–6703. DOI: 10.1021/j100078a009.

[8] Gordon Sproul. 'Electronegativity and Bond Type. 3. Origins of Bond Type'. In: *The Journal of Physical Chemistry* 98.50 (Dec. 1994), pp. 13221–13224. DOI: 10.1021/j100101a023.

[9] Chen Wang et al. 'Toughness enhancement of nanostructured hard coatings: Design strategies and toughness measurement techniques'. In: *Surface and Coatings Technology* 257 (Oct. 2014), pp. 206–212. DOI: 10.1016/j.surfcoat.2014.08.018.

[10] Yongjun Tian, Bo Xu and Zhisheng Zhao. 'Microscopic theory of hardness and design of novel superhard crystals'. In: *International Journal of Refractory Metals and Hard Materials* 33 (July 2012), pp. 93–106. DOI: 10.1016/j.ijrmhm.2012.02.021.

[11] J Haines, JM Léger and G Bocquillon. 'Synthesis and Design of Superhard Materials'. In: *Annual Review of Materials Research* 31.1 (Aug. 2001), pp. 1–23. DOI: 10.1146/annurev.matsci.31.1.1.

[12] R.L Fleischer. 'Substitutional solution hardening'. In: *Acta Metallurgica* 11.3 (Mar. 1963), pp. 203–209. DOI: 10.1016/0001-6160(63)90213-x.

[13] Timothy J. Rupert, Jonathan C. Trenkle and Christopher A. Schuh. 'Enhanced solid solution effects on the strength of nanocrystalline alloys'. In: *Acta Materialia* 59.4 (Feb. 2011), pp. 1619–1631. DOI: 10.1016/j.actamat.2010.11.026.

[14] G.P.M. Leyson, L.G. Hector and W.A. Curtin. 'Solute strengthening from first principles and application to aluminum alloys'. In: *Acta Materialia* 60.9 (May 2012), pp. 3873–3884. DOI: 10.1016/j.actamat.2012.03.037.

[15] Duancheng Ma et al. 'Computationally efficient and quantitatively accurate multiscale simulation of solid-solution strengthening by ab initio calculation'. In: *Acta Materialia* 85 (Feb. 2015), pp. 53–66. DOI: 10.1016/j.actamat.2014.10.044.

[16] Faming Gao. 'Hardness of cubic solid solutions'. In: *Scientific Reports* 7.1 (Jan. 2017). DOI: 10.1038/srep40276.

[17] S.F. Pugh. 'XCII. Relations between the elastic moduli and the plastic properties of polycrystalline pure metals'. In: *The London, Edinburgh, and Dublin Philosophical Magazine and Journal of Science* 45.367 (Aug. 1954), pp. 823–843. DOI: 10.1080/14786440808520496.

[18] D. G. Pettifor. 'Theoretical predictions of structure and related properties of intermetallics'. In: *Materials Science and Technology* 8.4 (Apr. 1992), pp. 345–349. DOI: 10.1179/mst.1992.8.4.345.

[19] Antonin Šimůnek. 'How to estimate hardness of crystals on a pocket calculator'. In: *Physical Review B* 75.17 (May 2007). DOI: 10.1103/physrevb.75.172108.

[20] D.G. Sangiovanni, L. Hultman and V. Chirita. 'Supertoughening in B1 transition metal nitride alloys by increased valence electron concentration'. In: *Acta Materialia* 59.5 (Mar. 2011), pp. 2121–2134. DOI: 10.1016/j.actamat.2010.12.013.

[21] Keyan Li et al. 'Electronegativity Identification of Novel Superhard Materials'. In: *Physical Review Letters* 100.23 (June 2008). DOI: 10.1103/physrevlett.100.235504.

[22] Andriy O. Lyakhov and Artem R. Oganov. 'Evolutionary search for superhard materials: Methodology and applications to forms of carbon and TiO2'. In: *Physical Review B* 84.9 (Sept. 2011). DOI: 10.1103/physrevb.84.092103.

[23] Xing-Qiu Chen et al. 'Modeling hardness of polycrystalline materials and bulk metallic glasses'. In: *Intermetallics* 19.9 (Sept. 2011), pp. 1275–1281. DOI: 10.1016/j.intermet.2011.03.026.

[24] A. A. Griffith. 'The Phenomena of Rupture and Flow in Solids'. In: *Philosophical Transactions of the Royal Society A: Mathematical, Physical and Engineering Sciences* 221.582-593 (Jan. 1921), pp. 163–198. DOI: 10.1098/rsta.1921.0006.

[25] JIAN-GANG GUO, LI-JUN ZHOU and YA-PU ZHAO. 'SIZE-DEPENDENT ELASTIC MODULUS AND FRACTURE TOUGHNESS OF THE NANOFILM WITH SURFACE EFFECTS'. In: *Surface Review and Letters* 15.05 (Oct. 2008), pp. 599–603. DOI: 10.1142/s0218625x08011901.

[26] James S. K.-L. Gibson et al. 'From quantum to continuum mechanics: studying the fracture toughness of transition metal nitrides and oxynitrides'. In: *Materials Research Letters* 6.2 (Dec. 2017), pp. 142–151. DOI: 10.1080/21663831.2017.1414081.

[27] Haiyang Niu, Shiwei Niu and Artem R. Oganov. 'Simple and accurate model of fracture toughness of solids'. In: (15th May 2018). arXiv: http://arxiv.org/abs/1805.05820v1 [cond-mat.mtrl-sci].

[28] R Hill. 'The Elastic Behaviour of a Crystalline Aggregate'. In: *Proceedings of the Physical Society. Section A* 65.5 (May 1952), pp. 349–354. DOI: 10.1088/0370-1298/65/5/307.

[29] Woldemar Voigt. *Lehrbuch der Kristallphysik*. ViewegTeubner Verlag, 1966. DOI: 10.1007/978-3-663-15884-4.

[30] Robert O. Ritchie. 'The conflicts between strength and toughness'. In: *Nature Materials* 10.11 (Nov. 2011), pp. 817–822. DOI: 10.1038/nmat3115.

[31] Beatriz Cordero et al. 'Covalent radii revisited'. In: *Dalton Transactions* 21 (2008), p. 2832. DOI: 10.1039/b801115j.

[32] Charles E. Mortimer, Ulrich Müller and Johannes Beck. *Chemie*. Thieme Georg Verlag, 7th Oct. 2015. 720 pp. ISBN: 3134843129. URL: https://www.ebook.de/de/product/24265615/charles_e_mortimer_ulrich_mueller_johannes_beck_chemie.html.

[33] Antonin Šimůnek and Jiri Vackar. 'Hardness of Covalent and Ionic Crystals: First-Principle Calculations'. In: *Physical Review Letters* 96.8 (Mar. 2006). DOI: 10.1103/physrevlett.96.085501.

[34] P.H. Mayrhofer et al. 'Protective Transition Metal Nitride Coatings'. In: *Comprehensive Materials Processing*. Elsevier, 2014, pp. 355–388. DOI: 10.1016/b978-0-08-096532-1.00423-4.

[35] Liangcai Zhou, David Holec and Paul H. Mayrhofer. 'First-principles study of elastic properties of cubic Cr1-xAlxN alloys'. In: *Journal of Applied Physics* 113.4 (Jan. 2013), p. 043511. DOI: 10.1063/1.4789378.

[36] S. Zhang et al. 'Elastic constants and critical thicknesses of ScGaN and ScAlN'. In: *Journal of Applied Physics* 114.24 (Dec. 2013), p. 243516. DOI: 10.1063/1.4848036.

[37] Erjun Zhao et al. 'Structural, mechanical and electronic properties of 4d transition metal mononitrides by first-principles'. In: *Computational Materials Science* 47.4 (Feb. 2010), pp. 1064–1071. DOI: 10.1016/j.commatsci.2009.12.011.

[38] Erjun Zhao and Zhijian Wu. 'Electronic and mechanical properties of 5d transition metal mononitrides via first principles'. In: *Journal of Solid State Chemistry* 181.10 (Oct. 2008), pp. 2814–2827. DOI: 10.1016/j.jssc.2008.07.022.

[39] Xiang Po Du, Yuan Xu Wang and V. C. Lo. 'Investigation of tetragonal ReN2 and WN2 with high shear moduli from first-principles calculations'. In: *Physics Letters A* 374.25 (May 2010), pp. 2569–2574. DOI: 10.1016/j.physleta.2010.04.020.

[40] Shigenobu Ogata and Ju Li. 'Toughness scale from first principles'. In: *Journal of Applied Physics* 106.11 (Dec. 2009), p. 113534. DOI: 10.1063/1.3267158.

[41] David Holec and Paul H. Mayrhofer. 'Surface energies of AlN allotropes from first principles'. In: *Scripta Materialia* 67.9 (Nov. 2012), pp. 760–762. DOI: 10.1016/j.scriptamat.2012.07.027.

[42] David Holec et al. 'Trends in the elastic response of binary early transition metal nitrides'. In: *Physical Review B* 85.6 (Feb. 2012). DOI: 10.1103/physrevb.85.064101.

[43] P. Djemia et al. 'Structural and elastic properties of ternary metal nitrides TixTa1-xN alloys: First-principles calculations versus experiments'. In: *Surface and Coatings Technology* 215 (Jan. 2013), pp. 199–208. DOI: 10.1016/j.surfcoat.2012.09.059.

[44] W. Chen and J.Z. Jiang. 'Elastic properties and electronic structures of 4d- and 5d-transition metal mononitrides'. In: *Journal of Alloys and Compounds* 499.2 (June 2010), pp. 243–254. DOI: 10.1016/j.jallcom.2010.03.176.

[45] Liangcai Zhou, David Holec and Paul H Mayrhofer. 'Ab initiostudy of the alloying effect of transition metals on structure, stability and ductility of CrN'. In: *Journal of Physics D: Applied Physics* 46.36 (Aug. 2013), p. 365301. DOI: 10.1088/0022-3727/46/36/365301.

[46] Zhi-Gang Mei, Sumit Bhattacharya and Abdellatif M. Yacout. 'First-principles study of fracture toughness enhancement in transition metal nitrides'. In: *Surface and Coatings Technology* 357 (Jan. 2019), pp. 903–909. DOI: 10.1016/j.surfcoat.2018.10.102.

[47] Liangcai Zhou et al. 'Structural stability and thermodynamics of CrN magnetic phases fromab initiocalculations and experiment'. In: *Physical Review B* 90.18 (Nov. 2014). DOI: 10.1103/physrevb.90.184102.

[48] Wai Yuen Fu Colin J. Humphreys Siyuan Zhang David Holec and Michelle A. Moram. 'Tunable optoelectronic and ferroelectric properties in Sc-based III-nitrides'. In: *Journal of Applied Physics* (2013). DOI: [http://dx.doi.org/10.1063/1.4824179].

[49] S. K. R. Patil et al. 'Super hard cubic phases of period VI transition metal nitrides: First principles investigation'. In: *Thin Solid Films* 517.2 (Nov. 2008), pp. 824–827. DOI: 10.1016/j.tsf.2008.07.034.

[50] Ichiro Yonenaga, Toshiyuki Shima and Marcel H. F. Sluiter. 'Nano-Indentation Hardness and Elastic Moduli of Bulk Single-Crystal AlN'. In: *Japanese Journal of Applied Physics* 41.Part 1, No. 7A (July 2002), pp. 4620–4621. DOI: 10.1143/jjap.41.4620.

[51] David M. Teter. 'Computational Alchemy: The Search for New Superhard Materials'. In: *MRS Bulletin* 23.01 (Jan. 1998), pp. 22–27. DOI: 10.1557/s0883769400031420.

[52] F. Levy et al. 'Electronic states and mechanical properties in transition metal nitrides'. In: *Surface and Coatings Technology* 120-121 (Nov. 1999), pp. 284–290. DOI: 10.1016/s0257-8972(99)00498-3.

[53] H. Holleck. 'Material selection for hard coatings'. In: *Journal of Vacuum Science & Technology A: Vacuum, Surfaces, and Films* 4.6 (Nov. 1986), pp. 2661–2669. DOI: 10.1116/1.573700.

[54] D. F. Nelson, ed. *Second and Higher Order Elastic Constants*. Springer-Verlag, 1992. DOI: 10.1007/b44185.

[55] Roger Chang and L. J. Graham. 'Low-Temperature Elastic Properties of ZrC and TiC'. In: *Journal of Applied Physics* 37.10 (Sept. 1966), pp. 3778–3783. DOI: 10.1063/1.1707923.

[56] J. J. Gilman and B. W. Roberts. 'Elastic Constants of TiC and TiB2'. In: *Journal of Applied Physics* 32.7 (July 1961), pp. 1405–1405. DOI: 10.1063/1.1736249.

[57] Hui Li et al. 'Structural, elastic and electronic properties of transition metal carbides TMC (TM=Ti, Zr, Hf and Ta) from first-principles calculations'. In: *Solid State Communications* 151.8 (Apr. 2011), pp. 602–606. DOI: 10.1016/j.ssc.2011.02.005.

[58] W. Wolf et al. 'First-principles study of elastic and thermal properties of refractory carbides and nitrides'. In: *Philosophical Magazine B* 79.6 (June 1999), pp. 839–858. DOI: 10.1080/13642819908214844.

[59] Aimin Hao et al. 'First-principles investigations on electronic, elastic and thermodynamic properties of ZrC and ZrN under high pressure'. In: *Materials Chemistry and Physics* 129.1-2 (Sept. 2011), pp. 99–104. DOI: 10.1016/j.matchemphys.2011.03.060.

[60] Lailei Wu et al. 'The phase stability and mechanical properties of Nb–C system: Using first-principles calculations and nano-indentation'. In: *Journal of Alloys and Compounds* 561 (June 2013), pp. 220–227. DOI: 10.1016/j.jallcom.2013.01.200.

[61] YangZhen Liu et al. 'Elasticity, electronic properties and hardness of MoC investigated by first principles calculations'. In: *Physica B: Condensed Matter* 419 (June 2013), pp. 45–50. DOI: 10.1016/j.physb.2013.03.016.

[62] Hans K. Tönshoff. *Werkzeuge für die moderne Fertigung*. Expert-Verlag GmbH, 11th June 1993. 226 pp. ISBN: 3816907660. URL: https://www.ebook.de/de/product/4522842/hans_k_toenshoff_werkzeuge_fuer_die_moderne_fertigung.html.

[63] T.S Srivatsan et al. 'An investigation of the influence of powder particle size on microstructure and hardness of bulk samples of tungsten carbide'. In: *Powder Technology* 122.1 (Jan. 2002), pp. 54–60. DOI: 10.1016/s0032-5910(01)00391-6.

[64] Sankalp Kota et al. 'Synthesis and Characterization of an Alumina Forming Nanolaminated Boride: MoAlB'. In: *Scientific Reports* 6.1 (May 2016). DOI: 10.1038/srep26475.

[65] Vincent Moraes et al. 'Ab initio inspired design of ternary boride thin films'. In: *Scientific Reports* 8.1 (June 2018). DOI: 10.1038/s41598-018-27426-w.

[66] Yong Pan et al. 'Phase stability and mechanical properties of hafnium borides: A first-principles study'. In: *Computational Materials Science* 109 (Nov. 2015), pp. 1–6. DOI: 10.1016/j.commatsci.2015.06.030.

[67] Xianfeng Hao et al. 'Low-compressibility and hard materialsReB2andWB2: Prediction from first-principles study'. In: *Physical Review B* 74.22 (Dec. 2006). DOI: 10.1103/physrevb.74.224112.

[68] Wen Jie Zhao and Yuan Xu Wang. 'Structural, mechanical, and electronic properties of , TaB, , and IrB: First-principle calculations'. In: *Journal of Solid State Chemistry* 182.10 (Oct. 2009), pp. 2880–2886. DOI: 10.1016/j.jssc.2009.07.054.

[69] Fu-Zhi Dai and Yanchun Zhou. 'A Modified Theoretical Model of Intrinsic Hardness of Crystalline Solids'. In: *Scientific Reports* 6.1 (Sept. 2016). DOI: 10.1038/srep33085.

[70] Joseph B. Mann et al. 'Configuration Energies of the d-Block Elements'. In: *Journal of the American Chemical Society* 122.21 (May 2000), pp. 5132–5137. DOI: 10.1021/ja9928677.

[71] Huiyang Gou et al. 'Stability of MnB2 with AlB2-type structure revealed by first-principles calculations and experiments'. In: *Applied Physics Letters* 102.6 (Feb. 2013), p. 061906. DOI: 10.1063/1.4792273.

[72] Qinfen Gu, Günter Krauss and Walter Steurer. 'Transition Metal Borides: Superhard versus Ultra-incompressible'. In: *Advanced Materials* 20.19 (Oct. 2008), pp. 3620–3626. DOI: 10.1002/adma.200703025.

[73] Hsiu-Ying Chung et al. 'Correlation between hardness and elastic moduli of the ultraincompressible transition metal diborides RuB2, OsB2, and ReB2'. In: *Applied Physics Letters* 92.26 (June 2008), p. 261904. DOI: 10.1063/1.2946665.

[74] G V Lewis and C R A Catlow. 'Potential models for ionic oxides'. In: *Journal of Physics C: Solid State Physics* 18.6 (Feb. 1985), pp. 1149–1161. DOI: 10.1088/0022-3719/18/6/010.

[75] M. A. Caravaca et al. 'Ab initiostudy of the elastic properties of single and polycrystal TiO2, ZrO2and HfO2in the cotunnite structure'. In: *Journal of Physics: Condensed Matter* 21.1 (Dec. 2008), p. 015501. DOI: 10.1088/0953-8984/21/1/015501.

[76] Xian Zhang, Wenhua Gui and Qingfeng Zeng. 'First-principles study of structural, mechanical, and thermodynamic properties of cubic Y2O3 under high pressure'. In: *Ceramics International* 43.3 (Feb. 2017), pp. 3346–3355. DOI: 10.1016/j.ceramint.2016.11.176.

[77] Yan Zhang et al. 'A comparison study of the structural and mechanical properties of cubic, tetragonal, monoclinic, and three orthorhombic phases of ZrO 2'. In: *Journal of Alloys and Compounds* 749 (June 2018), pp. 283–292. DOI: 10.1016/j.jallcom.2018.03.253.

[78] G.P. Cousland et al. 'Mechanical properties of zirconia, doped and undoped yttria-stabilized cubic zirconia from first-principles'. In: *Journal of Physics and Chemistry of Solids* 122 (Nov. 2018), pp. 51–71. DOI: 10.1016/j.jpcs.2018.06.003.

[79] A. R. Oganov and A. O. Lyakhov. 'Towards the theory of hardness of materials'. In: *Journal of Superhard Materials* 32.3 (June 2010), pp. 143–147. DOI: 10.3103/s1063457610030019.

[80] J. Castaing et al. 'Plastic deformation of CoO single crystals'. In: *Revue de Physique Appliquée* 15.2 (1980), pp. 277–283. DOI: 10.1051/rphysap:01980001502027700.

[81] C. F. Conde et al. 'Microhardness tests in nickel oxide single crystals'. In: *Physica Status Solidi (a)* 33.1 (Jan. 1976), K25–K29. DOI: 10.1002/pssa.2210330154.

[82] A. Audouard, B. Pellissier and J. Castaing. 'Slip systems of Cu2O by Knoop hardness anisotropy measurement'. In: *Journal de Physique Lettres* 38.1 (1977), pp. 33–35. DOI: 10.1051/jphyslet:0197700380103300.

[83] H.-Y. Chung et al. 'Synthesis of Ultra-Incompressible Superhard Rhenium Diboride at Ambient Pressure'. In: *Science* 316.5823 (Apr. 2007), pp. 436–439. DOI: 10.1126/science.1139322.

[84] M. Born and P. Jordan. 'Zur Quantenmechanik'. In: *Zeitschrift fr Physik* 34.1 (Dec. 1925), pp. 858–888. DOI: 10.1007/bf01328531.

[85] Y. C. Wang and R. S. Lakes. 'Composites with Inclusions of Negative Bulk Modulus: Extreme Damping and Negative Poisson's Ratio'. In: *Journal of Composite Materials* 39.18 (Sept. 2005), pp. 1645–1657. DOI: 10.1177/0021998305051112.

[86] Vladimir L. Solozhenko et al. 'Synthesis of superhard cubic BC2N'. In: *Applied Physics Letters* 78.10 (Mar. 2001), pp. 1385–1387. DOI: 10.1063/1.1337623.

[87] Faming Gao et al. 'Hardness of Covalent Crystals'. In: *Physical Review Letters* 91.1 (July 2003). DOI: 10.1103/physrevlett.91.015502.

[88] A. M. Saul and W. J. Smith. 'Available Information on Be2C'. In: (Aug. 1956).

[89] Ulrich Vogt. 'Carbide, nitride and boride materials—Synthesis and processing'. In: *Journal of the European Ceramic Society* 18.6 (Jan. 1998), pp. 735–736. DOI: 10.1016/s0955-2219(98)00075-2.

[90] Wei Zhang, Giles E. Eperon and Henry J. Snaith. 'Metal halide perovskites for energy applications'. In: *Nature Energy* 1.6 (May 2016), p. 16048. DOI: 10.1038/nenergy.2016.48.

[91] H. Deng et al. 'Structure, mechanical and tribological properties of d.c. magnetron sputtered TiB2 and TiB2(N) thin films'. In: *Surface and Coatings Technology* 76-77 (Dec. 1995), pp. 609–614. DOI: 10.1016/0257-8972(95)02517-0.

[92] R. A. Andrievski. 'The-State-of-the-Art of Nanostructured High Melting Point Compound-Based Materials'. In: *Nanostructured Materials*. Springer Netherlands, 1998, pp. 263–282. DOI: 10.1007/978-94-011-5002-6_13.

[93] P. Rogl and L. Delong. 'New ternary transition metal borides containing uranium and rare earth elements'. In: *Journal of the Less Common Metals* 91.1 (May 1983), pp. 97–106. DOI: 10.1016/0022-5088(83)90099-1.

[94] Abdelmadjid Bouhemadou. 'Structural, electronic and elastic properties of Ti2TlC, Zr2TlC and Hf2TlC'. In: *Open Physics* 7.4 (Jan. 2009). DOI: 10.2478/s11534-009-0022-z.

[95] W. Jeitschko, H. Nowotny and F. Benesovsky. 'Carbides of formula T2MC'. In: *Journal of the Less Common Metals* 7.2 (Aug. 1964), pp. 133–138. DOI: 10.1016/0022-5088(64)90055-4.

[96] Keyan Li et al. 'Hardness of Inorganic Functional Materials'. In: *Reviews in Advanced Sciences and Engineering* 1.4 (Dec. 2012), pp. 265–279. DOI: 10.1166/rase.2012.1012.

[97] F. Torres et al. In: *Journal of Materials Science* 36.20 (2001), pp. 4961–4967. DOI: 10.1023/a:1011808926424.

[98] Bertrand Devouard Peter R. Buseck William T. Petuskey Herve Hubert Laurence A. J. Garvie and Paul F. McMillan. 'High-Pressure, High-Temperature Synthesis and Characterization of Boron Suboxide (B6O)'. In: *Chem. Mater.,* (1998). DOI: 10.1021/cm970433+.

[99] Duanwei He et al. 'Boron suboxide: As hard as cubic boron nitride'. In: *Applied Physics Letters* 81.4 (July 2002), pp. 643–645. DOI: 10.1063/1.1494860.

[100] Jianfu Li et al. 'Electronic structures, phase stability and hardness of technetium boride: First-principles calculation'. In: *Physica B: Condensed Matter* 405.22 (Nov. 2010), pp. 4659–4663. DOI: 10.1016/j.physb.2010.08.056.

[101] B. Aronsson et al. 'Borides of Rhenium and the Platinum Metals. The Crystal Structure of Re7B3, ReB3, Rh7B3, RhB˜1.1, IrB˜1.1 and PtB.' In: *Acta Chemica Scandinavica* 14 (1960), pp. 733–741. DOI: 10.3891/acta.chem.scand.14-0733.

[102] E Sterer et al. 'High-pressure x-ray studies of the UCo3B2compound and ambient magnetic properties'. In: *Journal of Physics: Condensed Matter* 14.44 (Oct. 2002), pp. 10619–10622. DOI: 10.1088/0953-8984/14/44/344.

[103] P. Villars et al. 'Be4B'. In: *Landolt-Börnstein - Group III Condensed Matter*. Springer Berlin Heidelberg, 2012, pp. 261–261. DOI: 10.1007/978-3-642-22847-6_192.

[104] Andreas Hermann et al. 'LiBeB: A predicted phase with structural and electronic peculiarities'. In: *Physical Review B* 86.1 (July 2012). DOI: 10.1103/physrevb.86.014104.

[105] A. Escudeiro Santana et al. 'The role of hcp-AlN on hardness behavior of Ti1-xAlxN nanocomposite during annealing'. In: *Thin Solid Films* 469-470 (Dec. 2004), pp. 339–344. DOI: 10.1016/j.tsf.2004.08.147.

[106] K. Kutschej et al. 'Structure, mechanical and tribological properties of sputtered Ti1–xAlxN coatings with $0.5 \leq x \leq 0.75$'. In: *Surface and Coatings Technology* 200.7 (Dec. 2005), pp. 2358–2365. DOI: 10.1016/j.surfcoat.2004.12.008.

[107] Li Chen et al. 'The influence of age-hardening on turning and milling performance of Ti–Al–N coated inserts'. In: *Surface and Coatings Technology* 202.21 (July 2008), pp. 5158–5161. DOI: 10.1016/j.surfcoat.2008.05.036.

[108] Ferenc Tasnádi et al. 'Significant elastic anisotropy in Ti1-xAlxN alloys'. In: *Applied Physics Letters* 97.23 (Dec. 2010), p. 231902. DOI: 10.1063/1.3524502.

[109] Ayako Kimura et al. 'Effects of Al content on hardness, lattice parameter and microstructure of Ti1-xAlxN films'. In: *Surface and Coatings Technology* 120-121 (Nov. 1999), pp. 438–441. DOI: 10.1016/s0257-8972(99)00491-0.

[110] J.C. Sánchez-López et al. 'Tribological behaviour at high temperature of hard CrAlN coatings doped with Y or Zr'. In: *Thin Solid Films* 550 (Jan. 2014), pp. 413–420. DOI: 10.1016/j.tsf.2013.10.041.

[111] G. Greczynski et al. 'Venting temperature determines surface chemistry of magnetron sputtered TiN films'. In: *Applied Physics Letters* 108.4 (Jan. 2016), p. 041603. DOI: 10.1063/1.4940974.

[112] F. F. Klimashin et al. 'Composition driven phase evolution and mechanical properties of Mo–Cr–N hard coatings'. In: *Journal of Applied Physics* 118.2 (July 2015), p. 025305. DOI: 10.1063/1.4926734.

[113] A.C. Fischer-Cripps. 'Critical review of analysis and interpretation of nanoindentation test data'. In: *Surface and Coatings Technology* 200.14-15 (Apr. 2006), pp. 4153–4165. DOI: 10.1016/j.surfcoat.2005.03.018.

[114] Anthony C. Fischer-Cripps. 'Nanoindentation Instrumentation'. In: *Nanoindentation*. Springer New York, 2011, pp. 199–211. DOI: 10.1007/978-1-4419-9872-9_11.

[115] F.F. Klimashin and P.H. Mayrhofer. 'Ab initio-guided development of super-hard Mo–Al–Cr–N coatings'. In: *Scripta Materialia* 140 (Nov. 2017), pp. 27–30. DOI: 10.1016/j.scriptamat.2017.06.052.

[116] P.H. Mayrhofer et al. 'High-entropy ceramic thin films A case study on transition metal diborides'. In: *Scripta Materialia* 149 (May 2018), pp. 93–97. DOI: 10.1016/j.scriptamat.2018.02.008.

[117] L. Xu et al. 'Separation of Zirconium and Hafnium: A Review'. In: *Energy Materials 2014*. John Wiley & Sons, Inc., May 2015, pp. 451–457. DOI: 10.1002/9781119027973.ch53.